Multiple-Taper Detection of Elastic Anisotropy in P-to-S and S-to-P Converted Seismic Waves

Jeffrey Park[1], Xiaoran Chen[2] and Vadim Levin[2]

[1]Dept. of Earth and Planetary Sciences, Yale Univ., New Haven, CT 06511, USA
[2]Dept. of Earth and Planetary Sciences, Rutgers Univ., New Brunswick, NJ 08904, USA

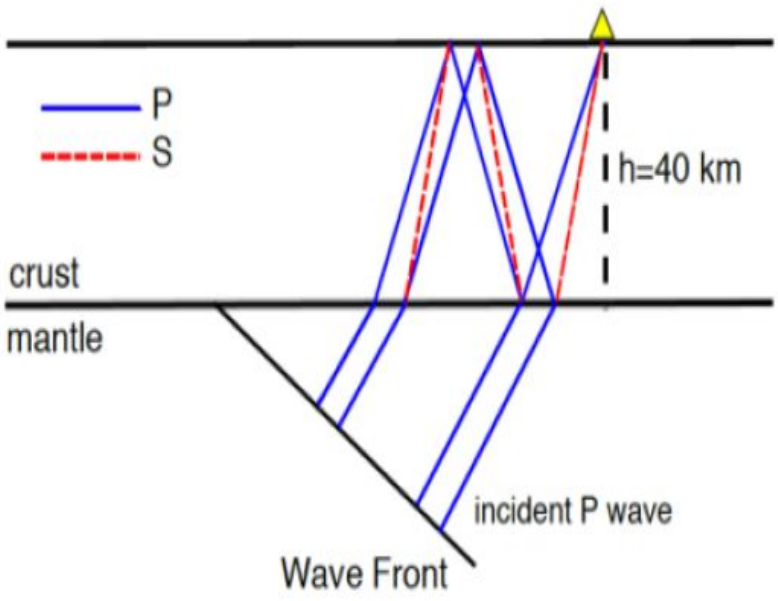

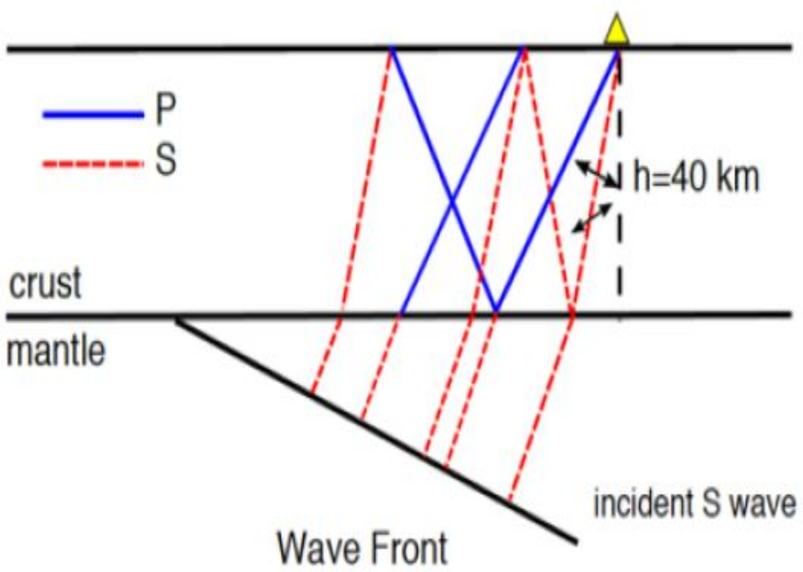

Why Should We Care??

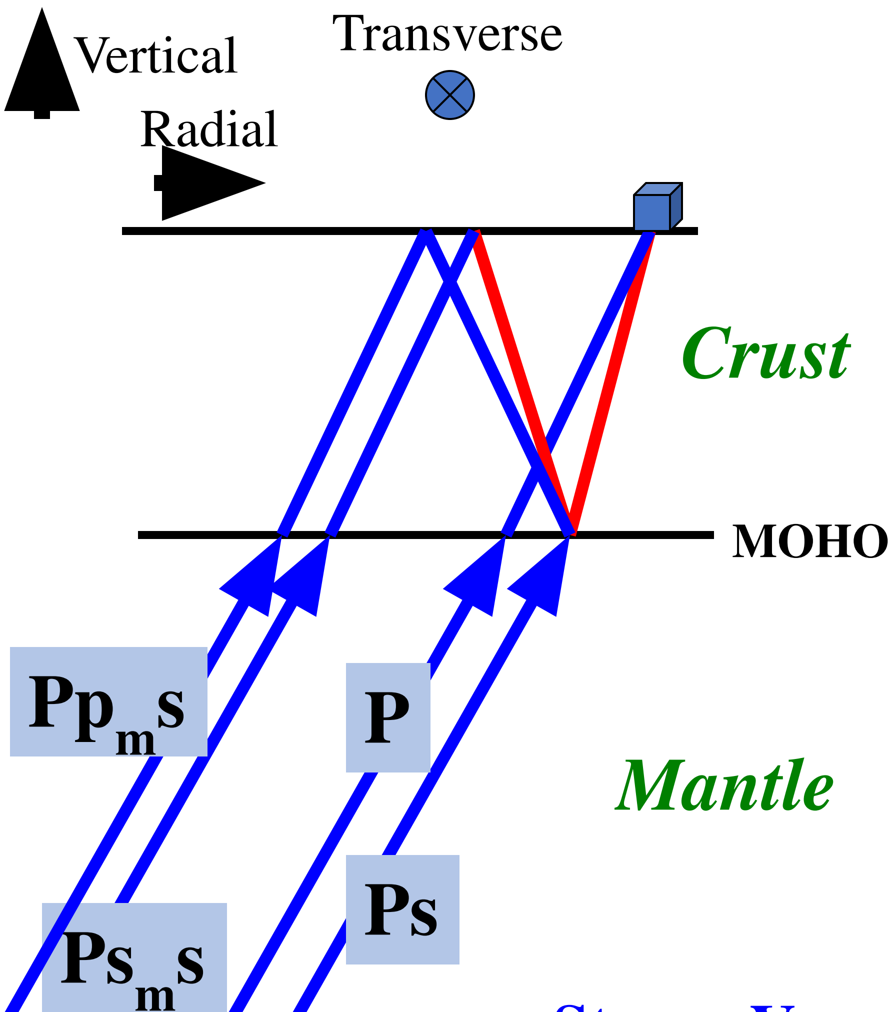

V_P = 5.5-6.5 km/s
V_S = 3.3-3.8 km/s

Light rock, extracted from mantle via partial melting

V_P = 7.5-8.5 km/s
V_S = 4.1-4.7 km/s

Dense rock with chemical composition similar to the stony meteorites

Strong V_P and V_S contrasts at MOHO induce significant P-to-SV conversions

Rock in the shallow mantle (<420 km) Contains 40-60% olivine $(Mg,Fe)_2SiO_4$

Olivine crystals are 20%+ anisotropic In elastic properties Aligned olivine in strained mantle rock can be 1-10% anisotropic in seismic wavespeed

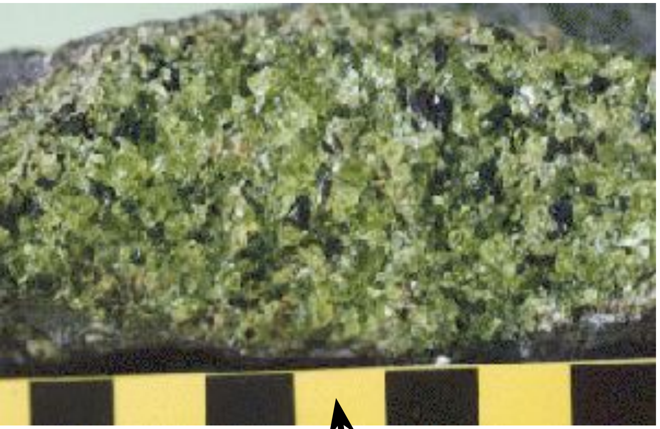

eduweb.brandonu.ca/~science/ Rocks/Rocks_lect.htm

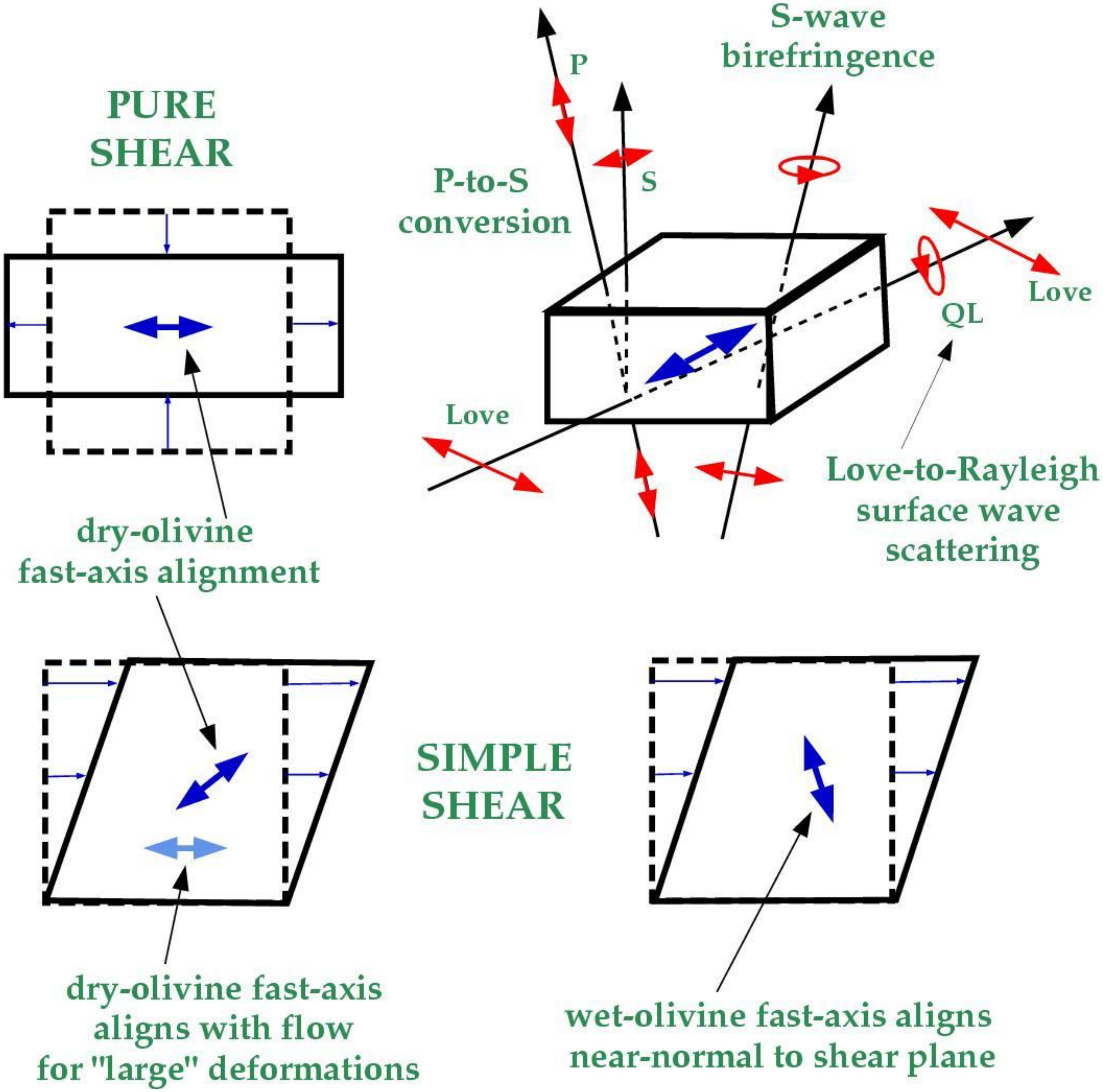

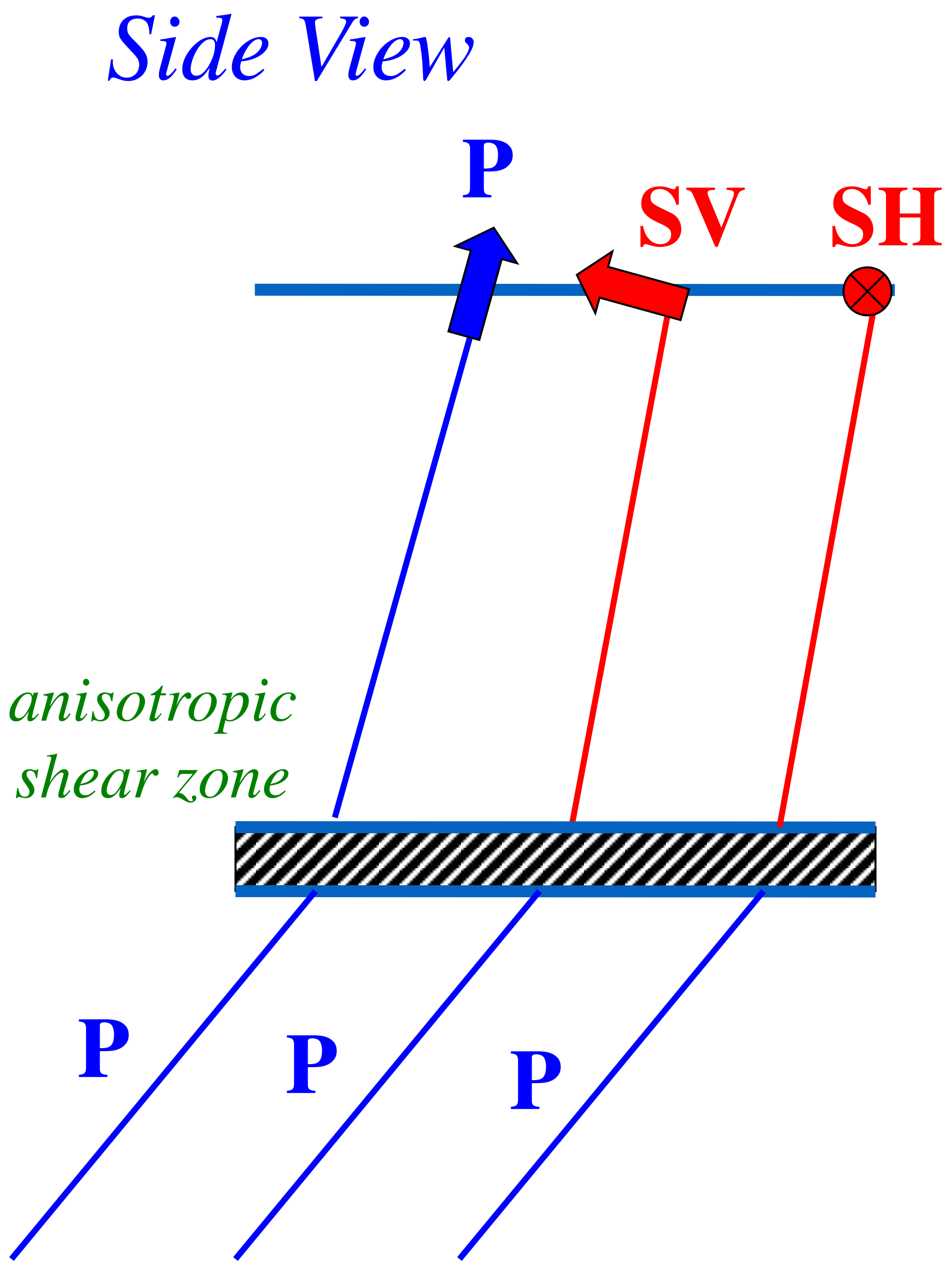
Side View
P
SV
SH
anisotropic
shear zone
P
P
P

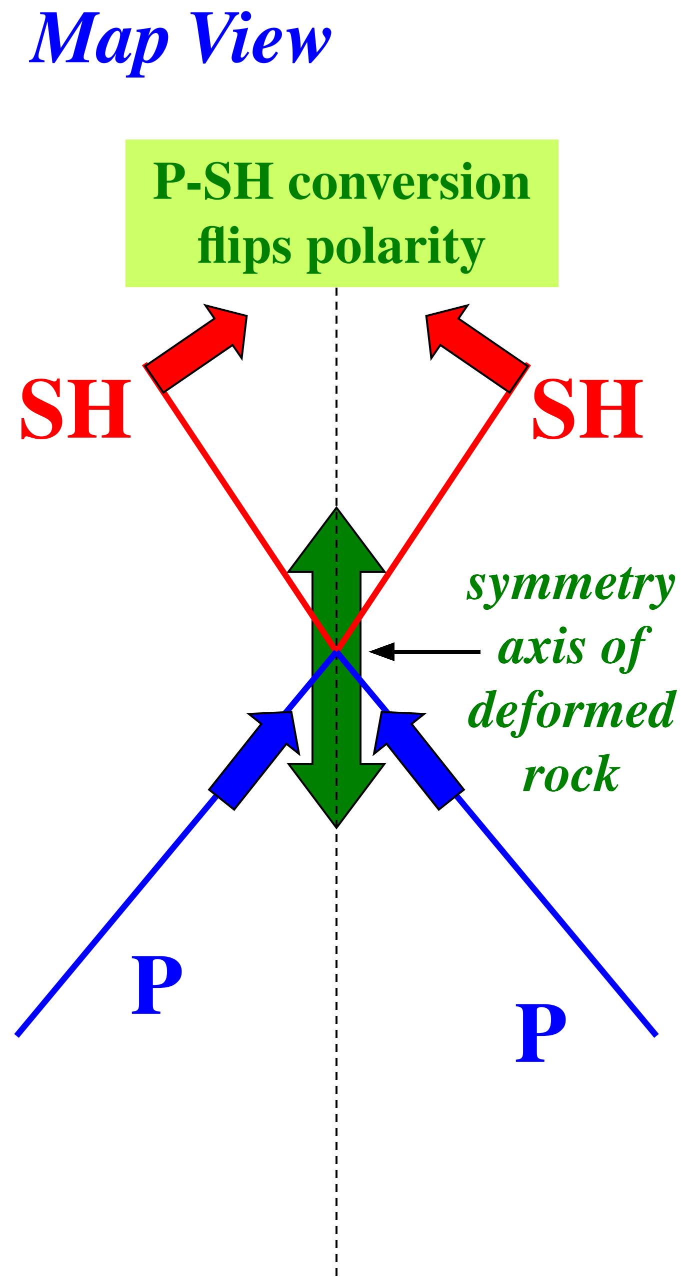
Map View
P-SH conversion
flips polarity
SH
SH
symmetry
axis of
deformed
rock
P
P

What Real Earthquake Data Looks Like

Station ARU: 7/14/89 Timor Event, mb=6.4

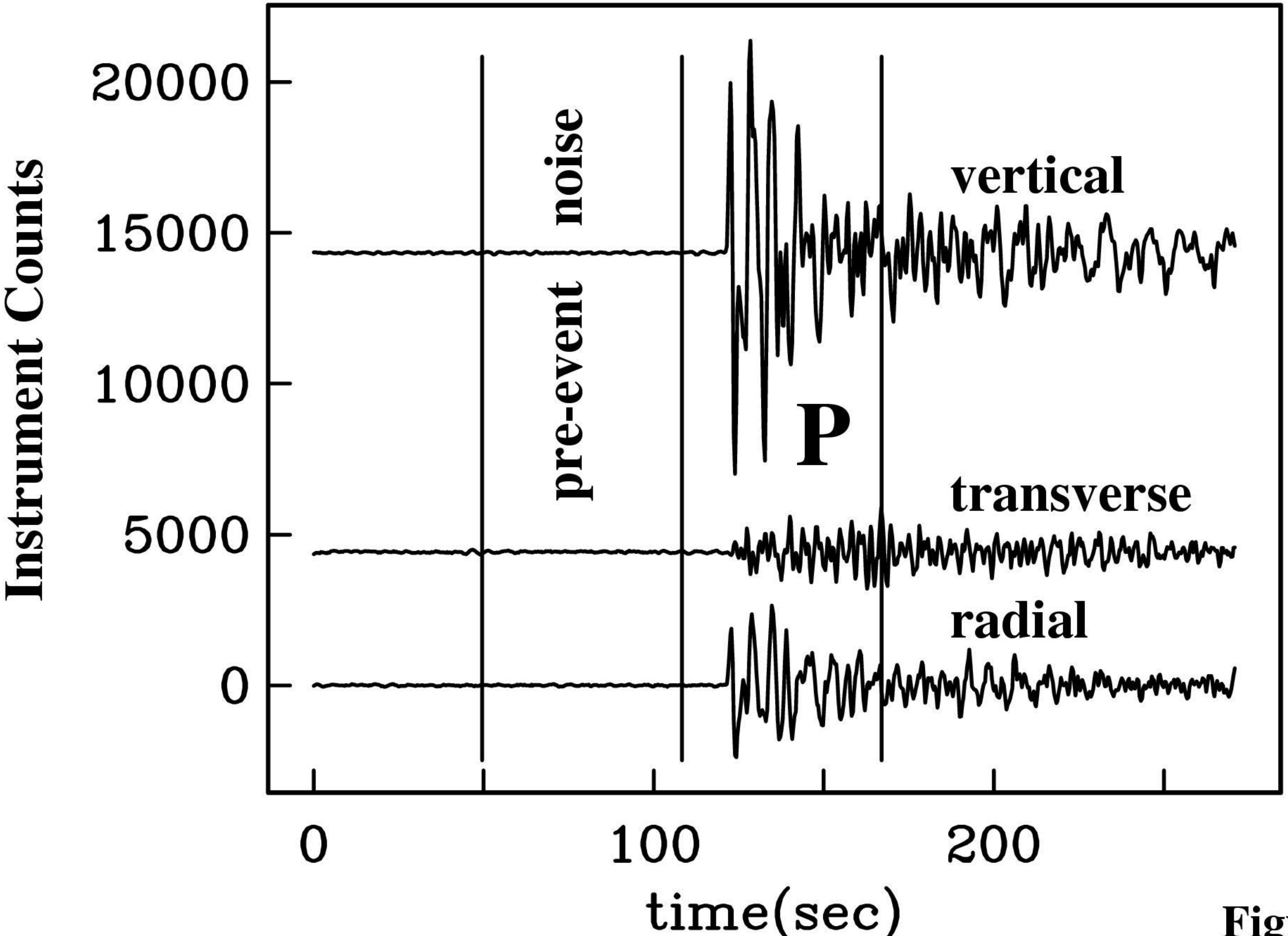

Figure 3

Need to deconvolve the components of the seismogram to remove the effect of the earthquake source

Receiver Functions (Phinney, 1964, Langston, 1981)

IDEA: for a vertically-incident P wave, most motion is on the vertical component

SO . . . . Use the vertical component record to predict the radial horizontal component, This approximately reconstructs the P-SV conversions in the form of a prediction filter

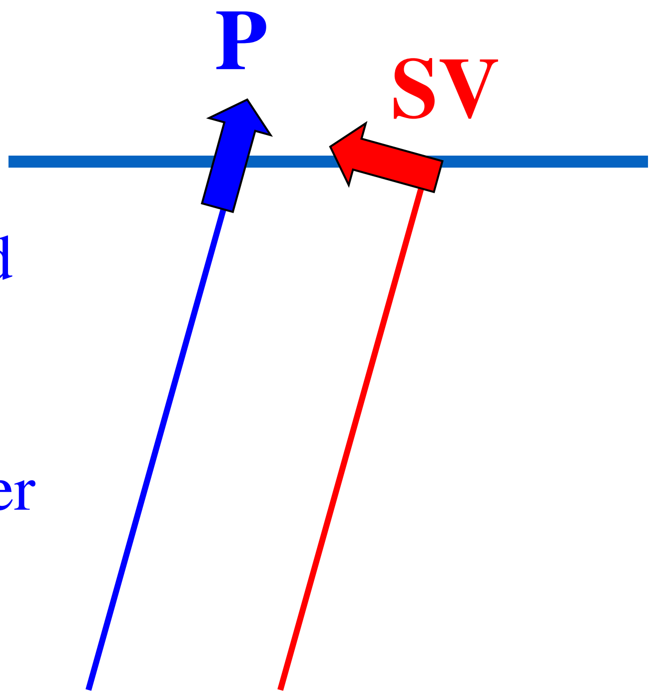

A Prediction Filter?

Time-Domain Deconvolution

$u_R(t) = \Sigma\, u_V(t-\tau)\, H(\tau)$
with M-point prediction filter
$H(0), H(\Delta t), H(2\Delta t) \ldots H((M-1)\Delta t)$

→ $\mathbf{G \cdot h = d}$

$$\mathbf{G} = \begin{pmatrix} u_V(0) & 0 & 0 & \ldots & 0 \\ u_V(\Delta t) & u_V(0) & 0 & \ldots & 0 \\ u_V(2\Delta t) & u_V(\Delta t) & u_V(0) & \ldots & 0 \\ u_V(3\Delta t) & u_V(2\Delta t) & u_V(\Delta t) & \ldots & 0 \\ u_V(4\Delta t) & u_V(3\Delta t) & u_V(2\Delta t) & \ldots & 0 \\ u_V(5\Delta t) & u_V(4\Delta t) & u_V(3\Delta t) & \ldots & 0 \\ \ldots\ldots & & & & \\ u_V((M-1)\Delta t) & u_V((M-2)\Delta t) & u_V((M-3)\Delta t) & \ldots & u_V(0) \end{pmatrix}$$

solution

$$\mathbf{h} = (\mathbf{G}^T \cdot \mathbf{G} + \sigma^2)^{-1} \cdot (\mathbf{G}^T \cdot \mathbf{d})$$

Has damping constant σ^2

Or compute a prediction filter H(f) in the frequency domain

Assumption: $u_R(t) = \Sigma\, u_V(t-\tau)\, H(\tau)$ ➡ $u_R(f) = u_V(f)H(f)$

$H(f) = u_R(f)/u_V(f)$ ➡ inverse FFT obtains H(t)

Problem: $u_R(f)$, $u_V(f)$ **are estimated from the DFT of the P-wave data, and their spectral ratio has high variance**

Typical solution: add a damping constant to the denominator (water-level trick)

$H(f) = u_R(f)/(u_V(f)+\sigma)$

Multitaper Receiver Function Estimate:

Eschew spectral ratios for cross-correlation (more stable!)

Treat $u_R(f)=H_R(f)u_V(f)$
$u_T(f)=H_T(f)u_V(f)$ as least-square estimates

HOW?

Take K statistically independent estimates of spectrum at f,

$\mathbf{U}_R(f) = [u_R^{(0)}(f), u_R^{(1)}(f), u_R^{(2)}(f), \ldots u_R^{(K-1)}(f)]$

$\mathbf{U}_T(f) = [u_T^{(0)}(f), u_T^{(1)}(f), u_T^{(2)}(f), \ldots u_T^{(K-1)}(f)]$

$\mathbf{U}_V(f) = [u_V^{(0)}(f), u_V^{(1)}(f), u_V^{(2)}(f), \ldots u_V^{(K-1)}(f)]$

and solve $\mathbf{U}_R(f) = H_R(f)\mathbf{U}_V(f)$ and $\mathbf{U}_T(f) = H_T(f)\mathbf{U}_V(f)$

as vector projections, e.g., $H_R(f) = \dfrac{(\mathbf{U}_V(f))^* \cdot \mathbf{U}_R(f)}{(\mathbf{U}_V(f))^* \cdot \mathbf{U}_V(f)}$

Denominator has lower variance
(2K statistical degrees of freedom)

Assume we have three time series of vertical, radial and transverse particle motion $[u_R(n\tau), u_T(n\tau), u_Z(n\tau)] = \{u_n^R, u_n^T, u_n^Z\}_{n=0}^{N-1}$ with sampling interval τ and duration $T = N\tau$. At each frequency f, the K multiple-taper spectrum estimates

$$Y_\gamma^{(k)}(f) = \sum_n u_n^\gamma w_n^{(k)} e^{i2\pi f n\tau}, \tag{1}$$

where $\{w_n^{(k)}\}_{n=0}^{N-1}$ is the Kth Slepian data taper for a user-chosen time-bandwidth product p. The $Y_\gamma^{(k)}(f)$ can be combined to form coherence estimates $C_R(f), C_T(f)$ between horizontal and vertical components:

$$\begin{aligned} C_R(f) &= \frac{\sum_{k=0}^{K-1} (Y_Z^{(k)}(f))^* Y_R^{(k)}(f)}{\left(\left(\sum_{k=0}^{K-1} (Y_R^{(k)}(f))^* Y_R^{(k)}(f)\right)\left(\sum_{k=0}^{K-1} (Y_Z^{(k)}(f))^* Y_Z^{(k)}(f)\right)\right)^{1/2}} \\ C_T(f) &= \frac{\sum_{k=0}^{K-1} (Y_Z^{(k)}(f))^* Y_T^{(k)}(f)}{\left(\left(\sum_{k=0}^{K-1} (Y_T^{(k)}(f))^* Y_T^{(k)}(f)\right)\left(\sum_{k=0}^{K-1} (Y_Z^{(k)}(f))^* Y_Z^{(k)}(f)\right)\right)^{1/2}} \end{aligned} \tag{2}$$

In the applications that follow, we fix time-bandwidth product $p = 2.5$ and $K = 3$, so that the $(C_R(f))^2$ and $(C_T(f))^2$ can, for locally-white spectral processes, be related to the F variance-ratio test with 2 and 4 degrees of freedom.

We identify the frequency-domain receiver functions $H_R(f), H_T(f)$ with the damped spectral correlation estimators

$$
\begin{aligned}
H_R(f) &= \frac{\sum_{k=0}^{K-1} (Y_Z^{(k)}(f))^* Y_R^{(k)}(f)}{\left(\left(\sum_{k=0}^{K-1} (Y_Z^{(k)})^* Y_Z^{(k)}\right) + S_o(f)\right)} \\
H_T(f) &= \frac{\sum_{k=0}^{K-1} (Y_Z^{(k)}(f))^* Y_T^{(k)}(f)}{\left(\left(\sum_{k=0}^{K-1} (Y_Z^{(k)})^* Y_Z^{(k)}\right) + S_o(f)\right)}
\end{aligned}
\qquad (3)
$$

The damping factor $S_o(f)$ is a spectrum estimate of the pre-event noise on the vertical component.

The variance of the RF scales with its squared amplitude

$$
\begin{aligned}
\mathrm{var}(H_R(f)) &= \left(\frac{1-(C_R(f))^2}{(K-1)(C_R(f))^2}\right) |H_R(f)|^2 \\
\mathrm{var}(H_T(f)) &= \left(\frac{1-(C_T(f))^2}{(K-1)(C_T(f))^2}\right) |H_T(f)|^2
\end{aligned}
\qquad (4)
$$

The formal uncertainty is small when coherence is near unity, and large for smaller coherences. For $(C_\gamma(f))^2 = 1/K$, the expectation for random noise, $\mathrm{var}(H_\gamma(f)) = |H_\gamma(f)|^2$.

We compute time-domain MTC receiver functions $H_R(t)$ and $H_T(t)$ via an inverse Fourier transform of $H_R(f)$ and $H_T(f)$. To avoid Gibbs-effect ringing in the RF, we lowpass the spectrum up to a user-specified cutoff frequency f_c with a cosine-squared function.

The coherence between horizontal and vertical is spotty!

Station ARU: 7/14/89 Timor Event, mb=6.4

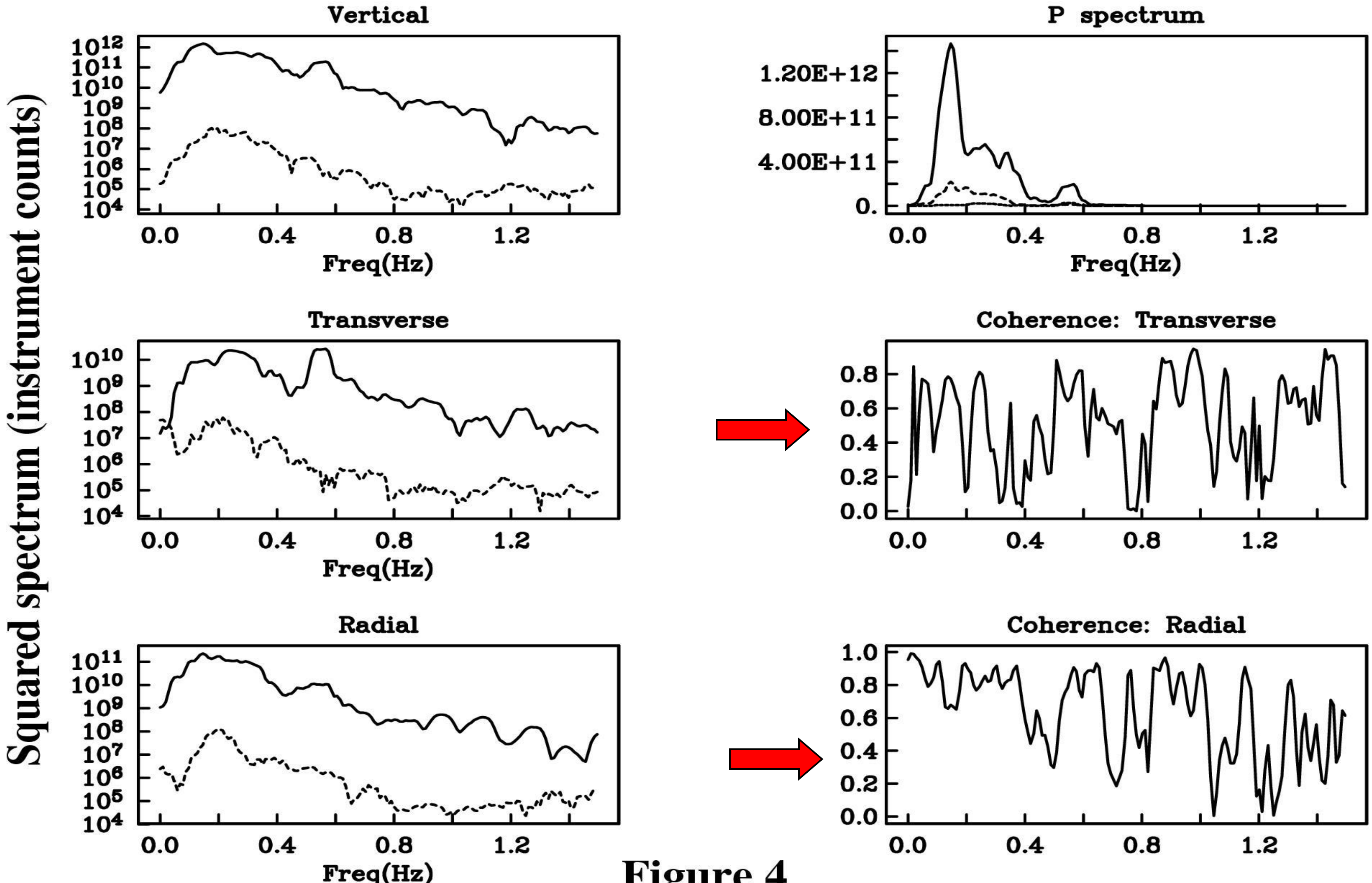

Figure 4

Station ARU: 7/14/89 Timor Event, mb=6.4

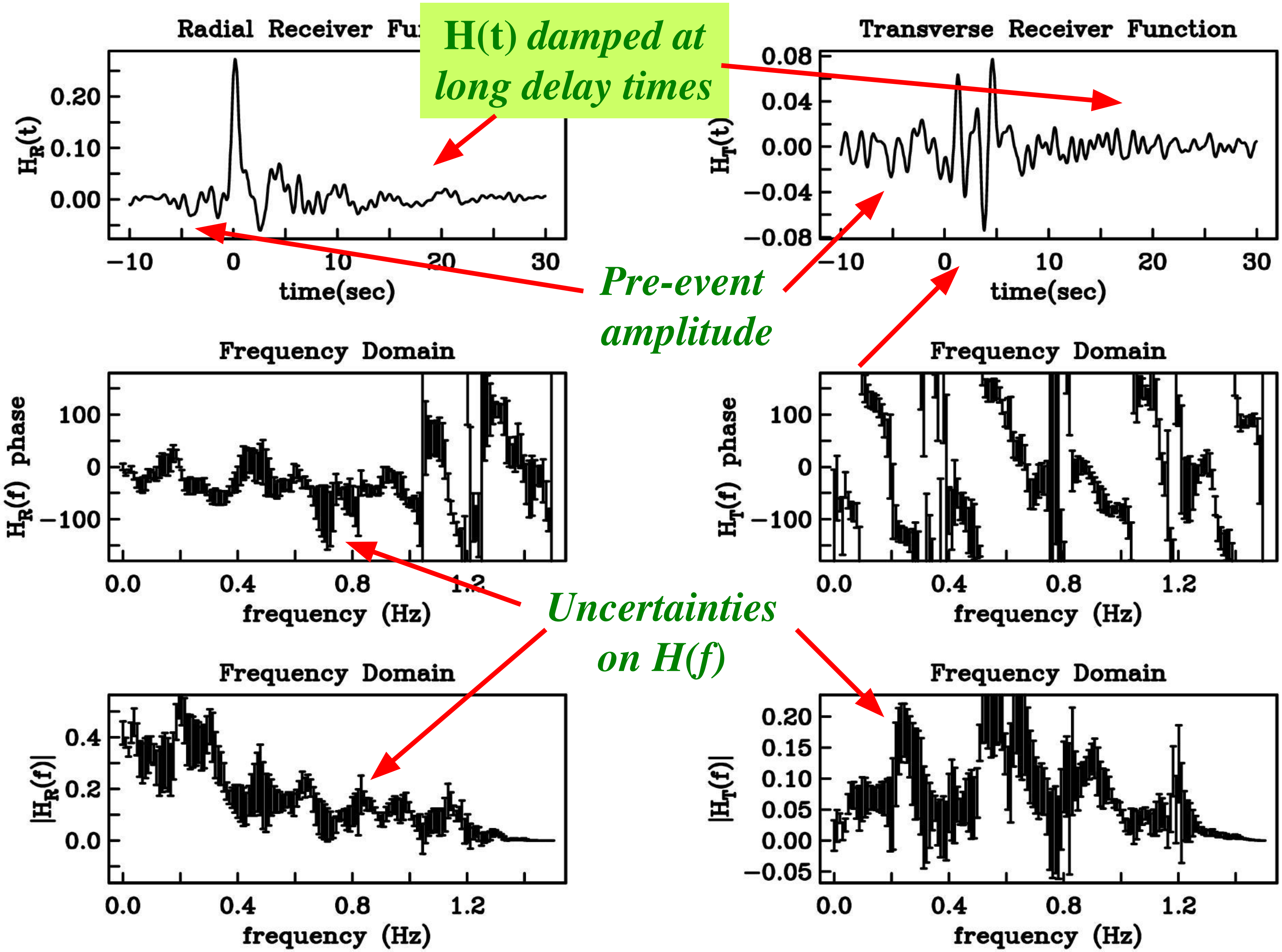

Uncertainties allow us to stack H(f) in a variance-weighted sum

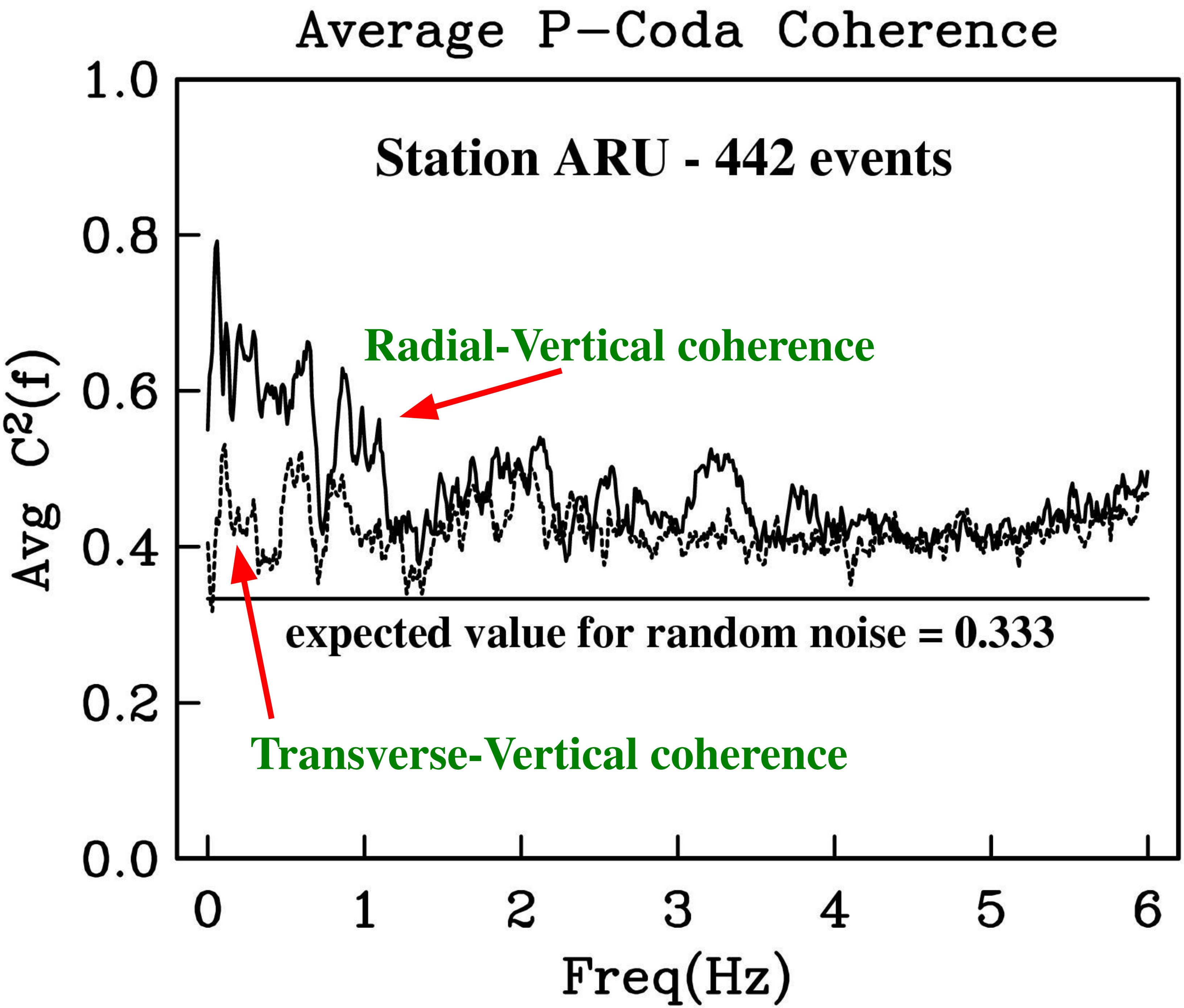

Average P-Coda Coherence
Station ARU - 442 events
Radial-Vertical coherence
Transverse-Vertical coherence
expected value for random noise = 0.333
Avg C²(f)
Freq(Hz)
1.0
0.8
0.6
0.4
0.2
0.0
0
1
2
3
4
5
6

Levin and Park (1998)
Time-domain deconvolution → ***Park and Levin (2000)***
Multiple-taper correlation

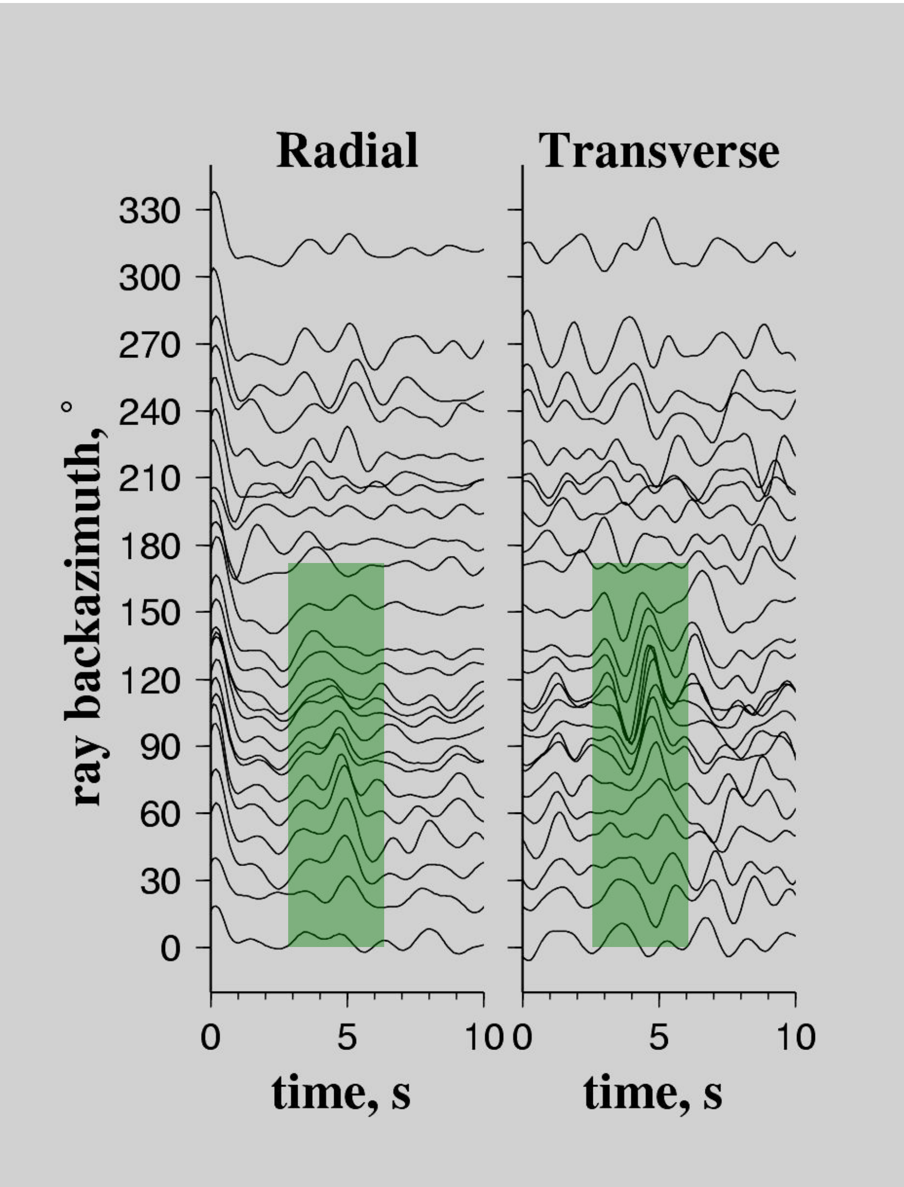

ARU: RF sweeps, 1989-98 data

Freq cutoff 1.5 Hz

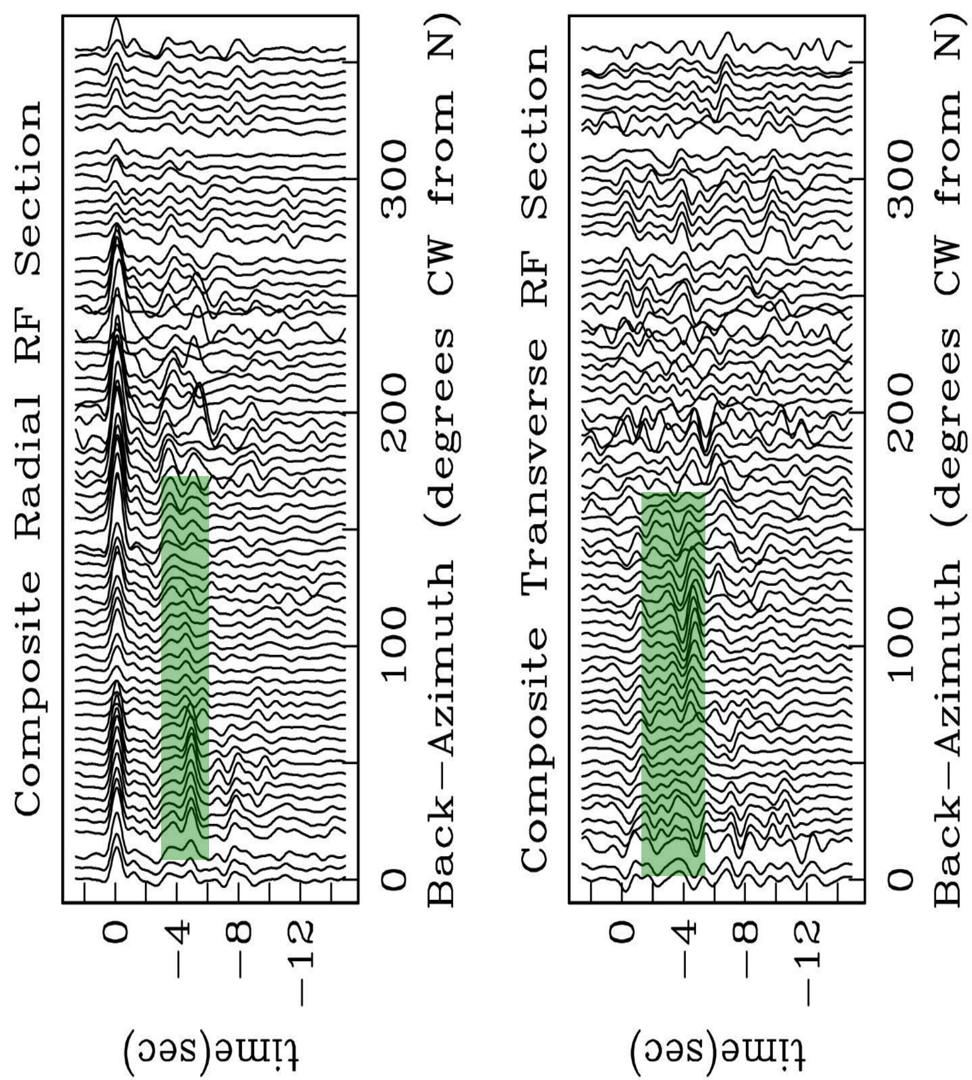

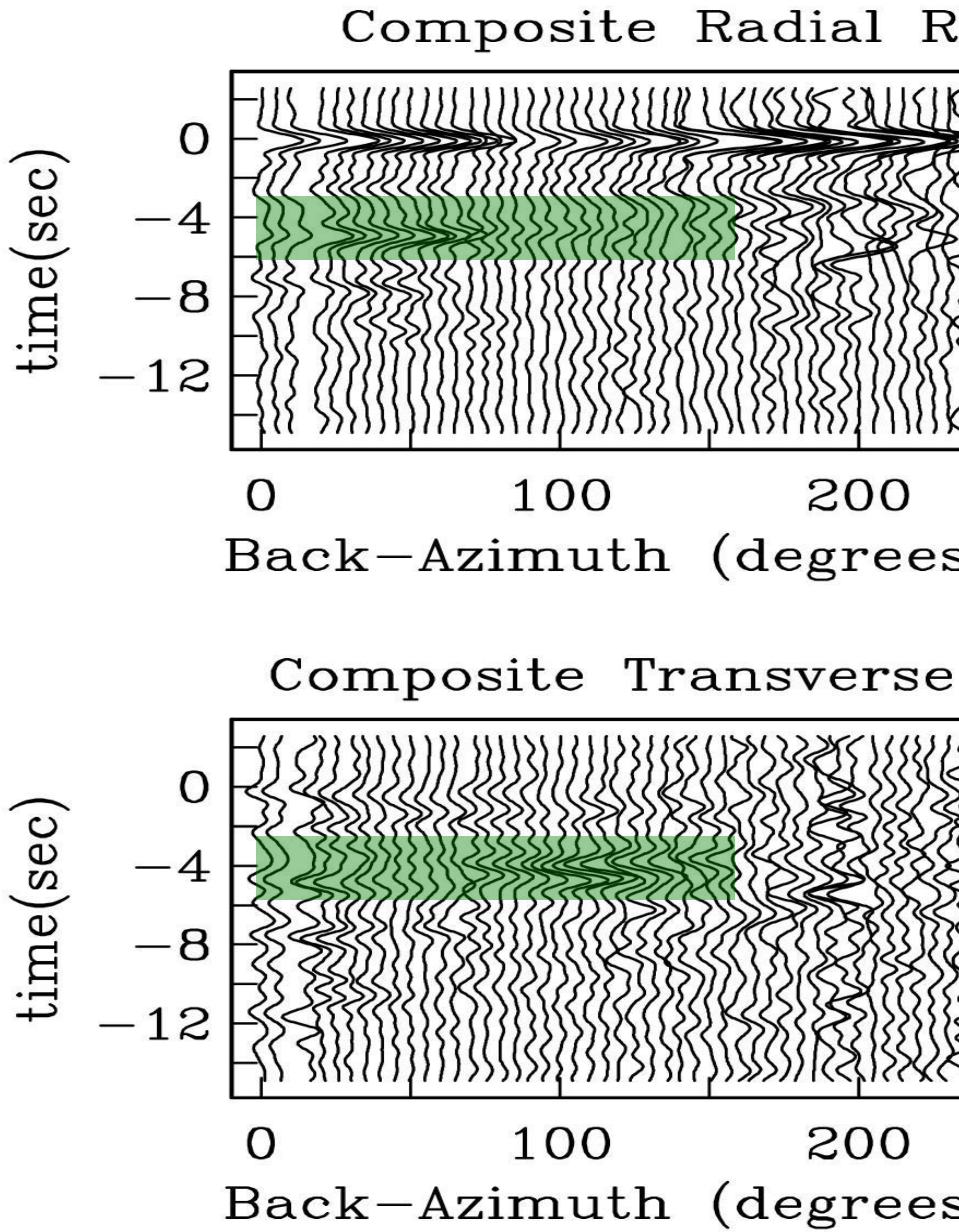

Composite Radial R
time(sec)
0
−4
−8
−12
0
100
200
Back−Azimuth (degrees
Composite Transverse
time(sec)
0
−4
−8
−12
0
100
200
Back−Azimuth (degrees

Geophysical Journal International

Geophys. J. Int. (2016) **207,** 512–527 doi: 10.1093/gji/ggw291
Advance Access publication 2016 August 1
GJI Seismology

Statistics and frequency-domain moveout for multiple-taper receiver functions

J. Park[1] and V. Levin[2]

[1] *Department of Geology and Geophysics, Y*
[2] *Department of Earth and Planetary Scienc*

Accepted 2016 July 28. Received 2016 July

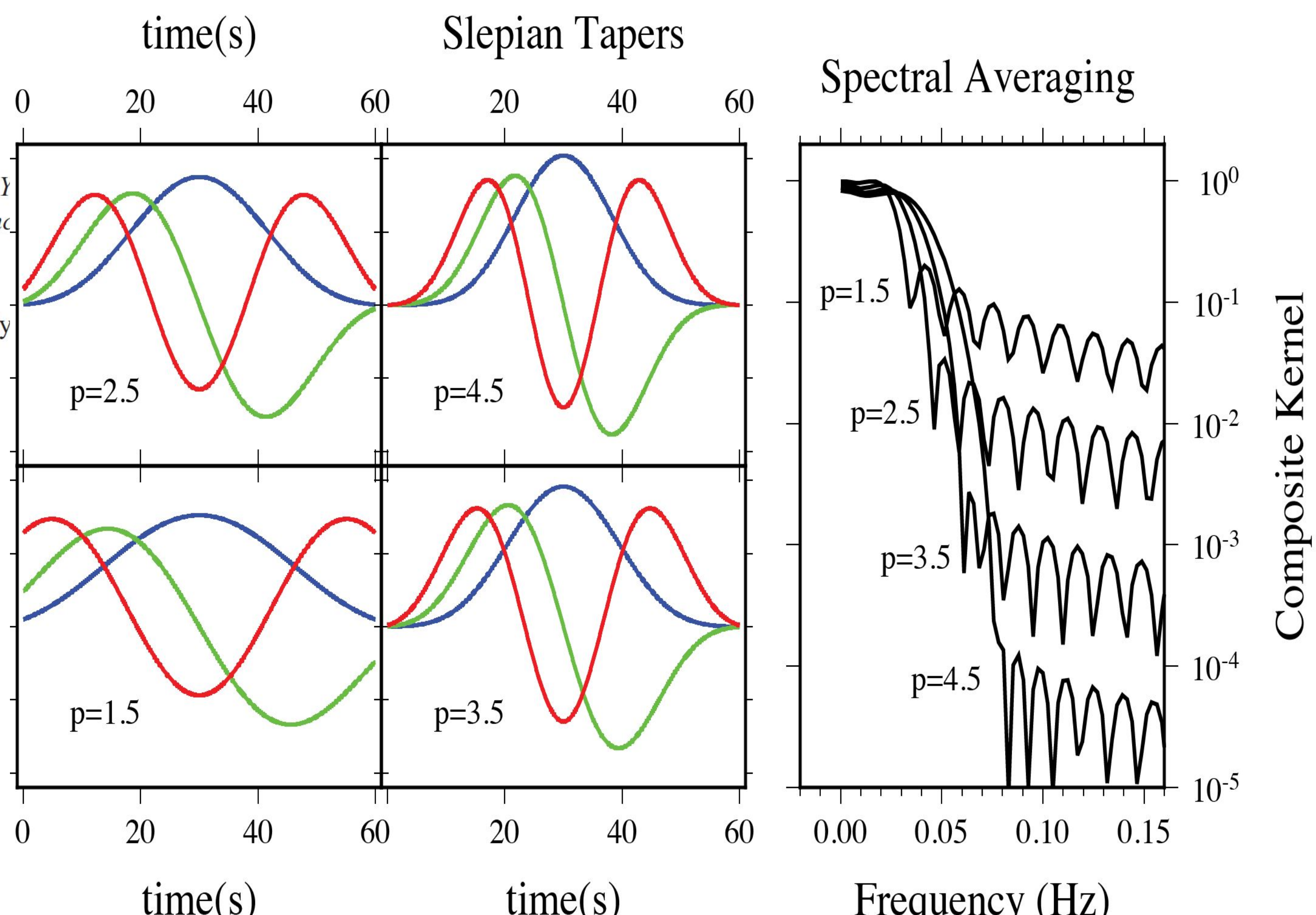

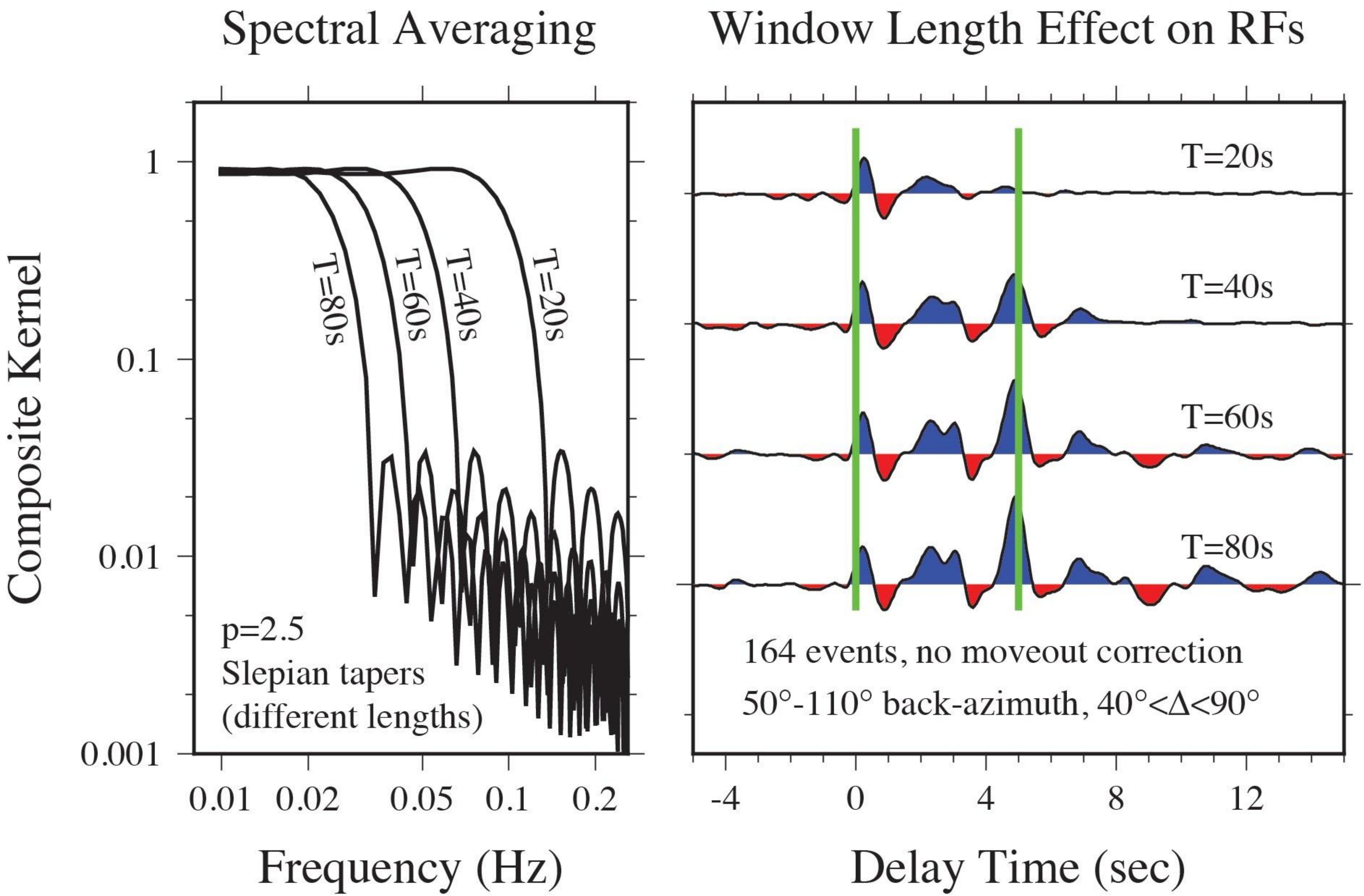

Spectral Averaging
Window Length Effect on RFs
Composite Kernel
1
0.1
0.01
0.001
T=80s
T=60s
T=40s
T=20s
p=2.5
Slepian tapers
(different lengths)
0.01
0.02
0.05
0.1
0.2
Frequency (Hz)
T=20s
T=40s
T=60s
T=80s
164 events, no moveout correction
50°-110° back-azimuth, 40°<Δ<90°
-4
0
4
8
12
Delay Time (sec)

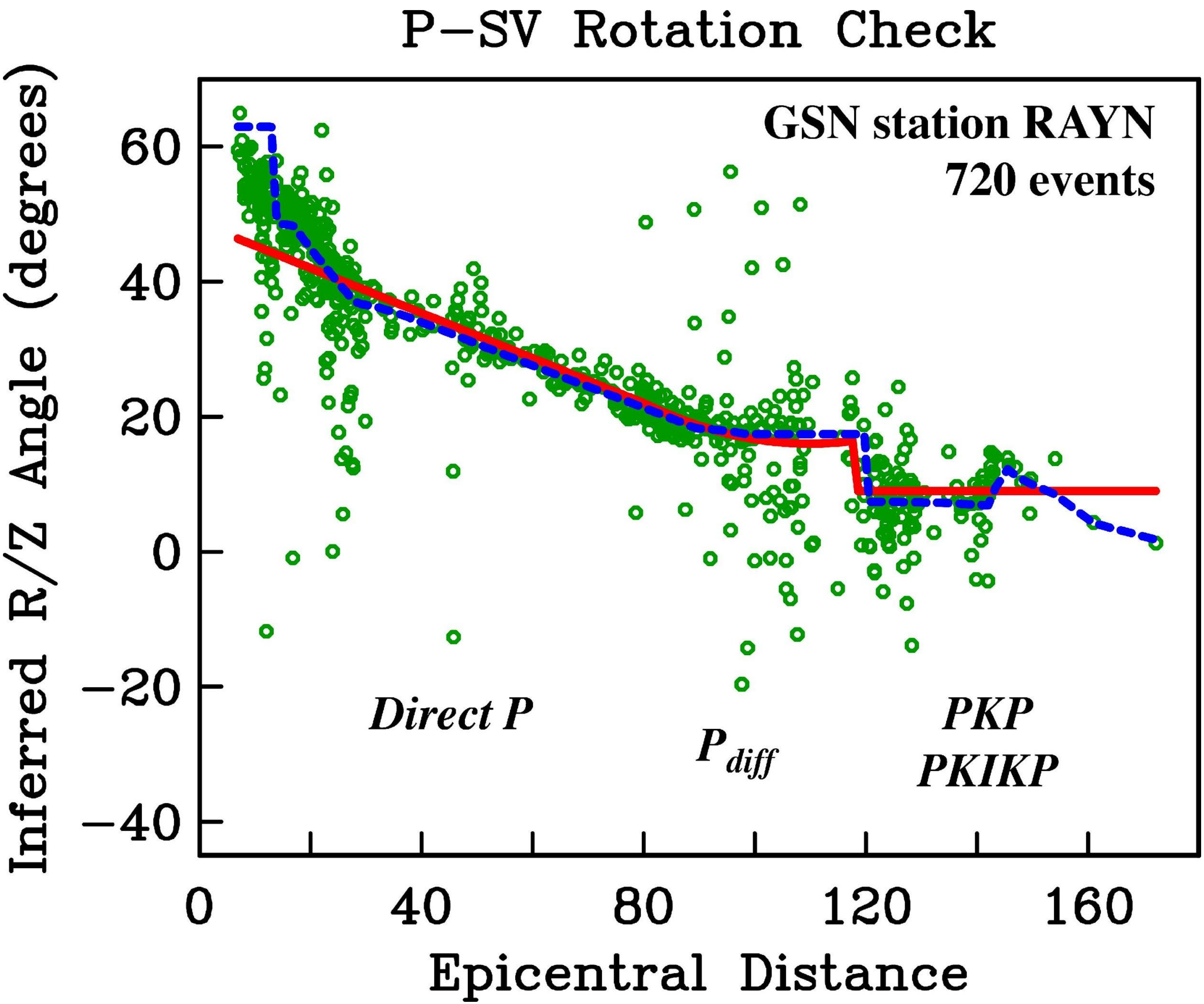
P-SV Rotation Check
GSN station RAYN
720 events
Inferred R/Z Angle (degrees)
60
40
20
0
−20
−40
Direct P
P_{diff}
PKP
PKIKP
0
40
80
120
160
Epicentral Distance

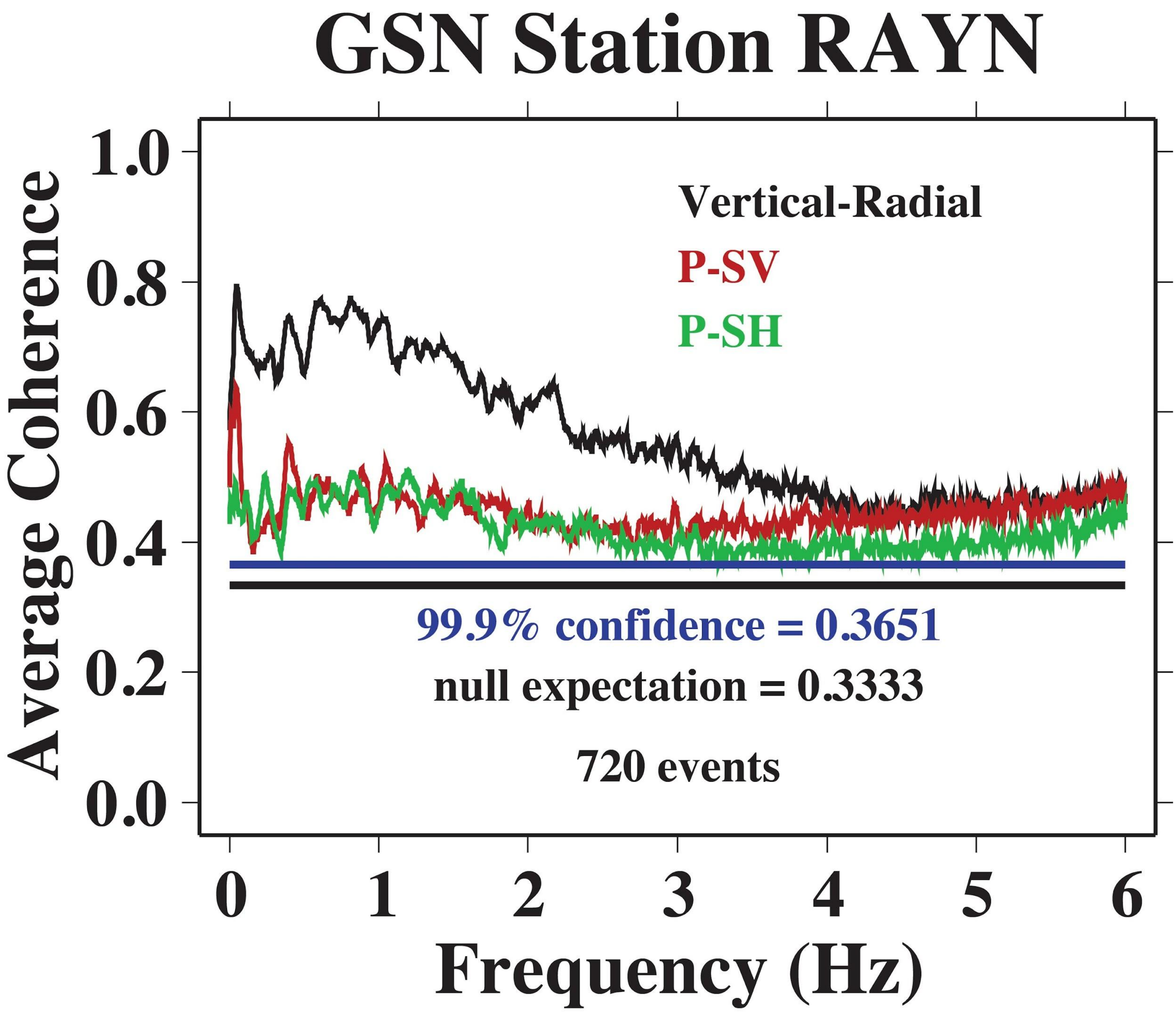
GSN Station RAYN
Average Coherence
1.0
0.8
0.6
0.4
0.2
0.0
Vertical-Radial
P-SV
P-SH
99.9% confidence = 0.3651
null expectation = 0.3333
720 events
0
1
2
3
4
5
6
Frequency (Hz)

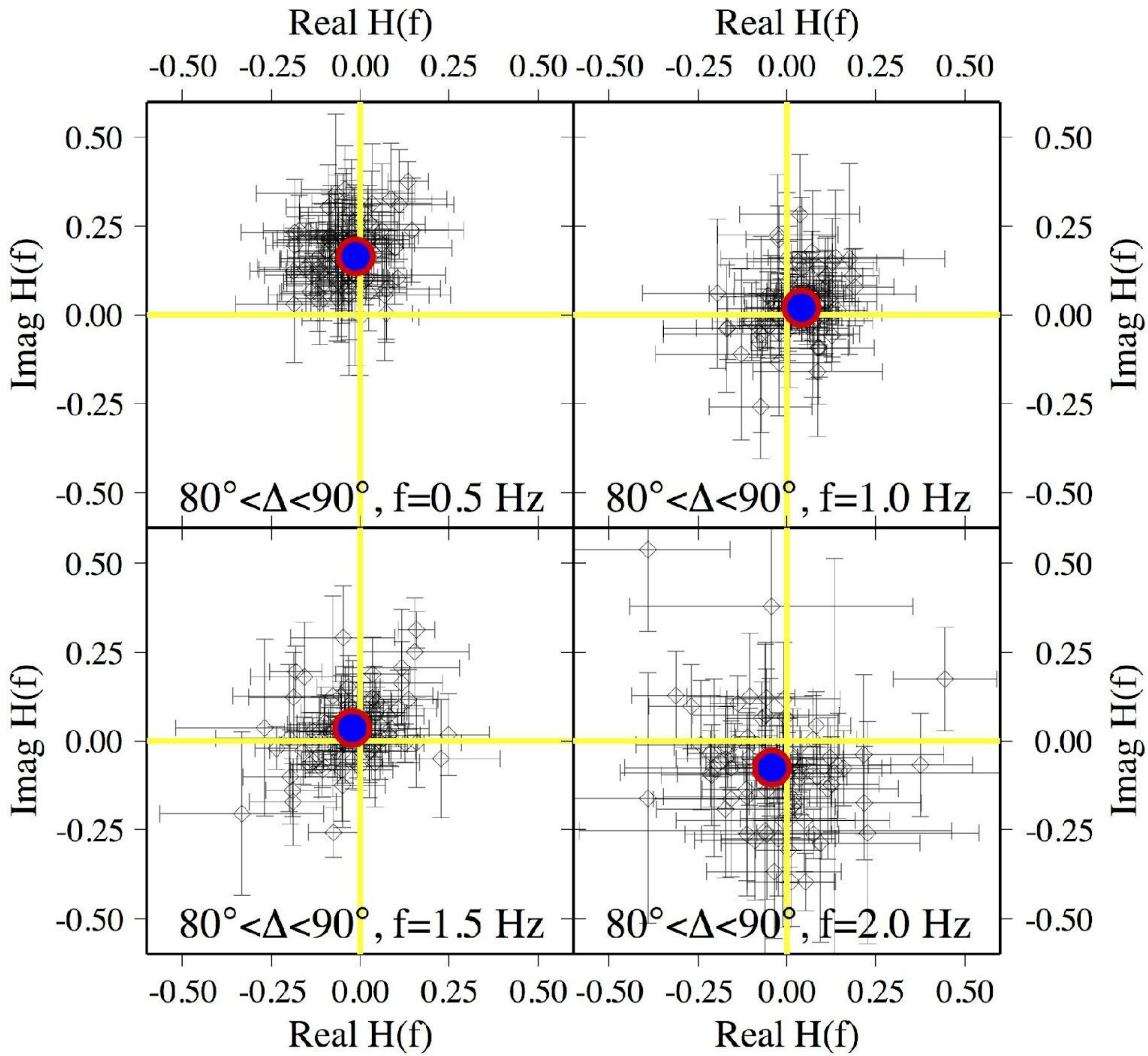
Real H(f)
-0.50
-0.25
0.00
0.25
0.50
Imag H(f)
80°<Δ<90°, f=0.5 Hz
80°<Δ<90°, f=1.0 Hz
80°<Δ<90°, f=1.5 Hz
80°<Δ<90°, f=2.0 Hz

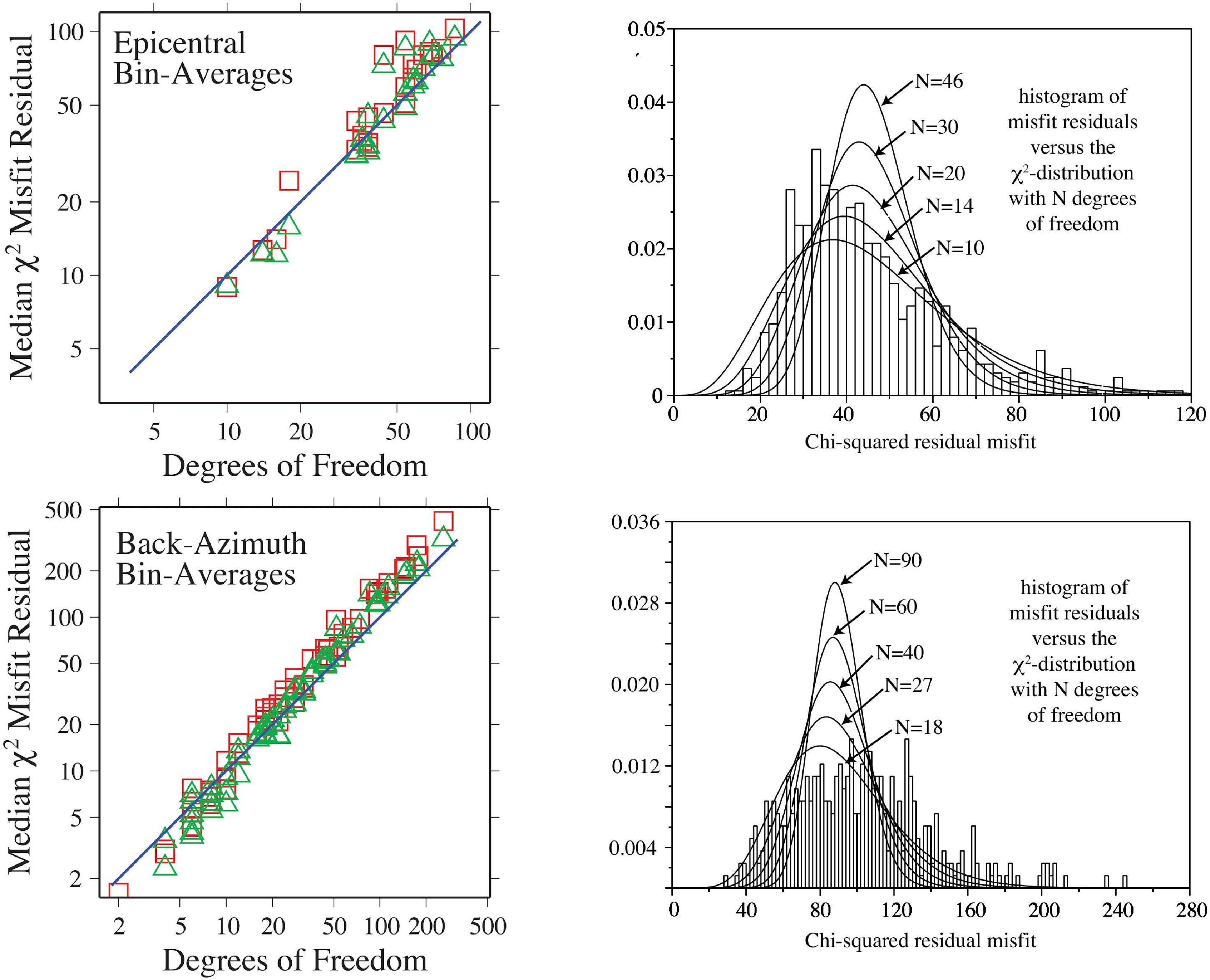

Epicentral
Bin-Averages
Median χ2 Misfit Residual
Degrees of Freedom
histogram of
misfit residuals
versus the
χ2-distribution
with N degrees
of freedom
N=46
N=30
N=20
N=14
N=10
Chi-squared residual misfit
Back-Azimuth
Bin-Averages
Median χ2 Misfit Residual
Degrees of Freedom
N=90
N=60
N=40
N=27
N=18
Chi-squared residual misfit

Moving-Window Migration

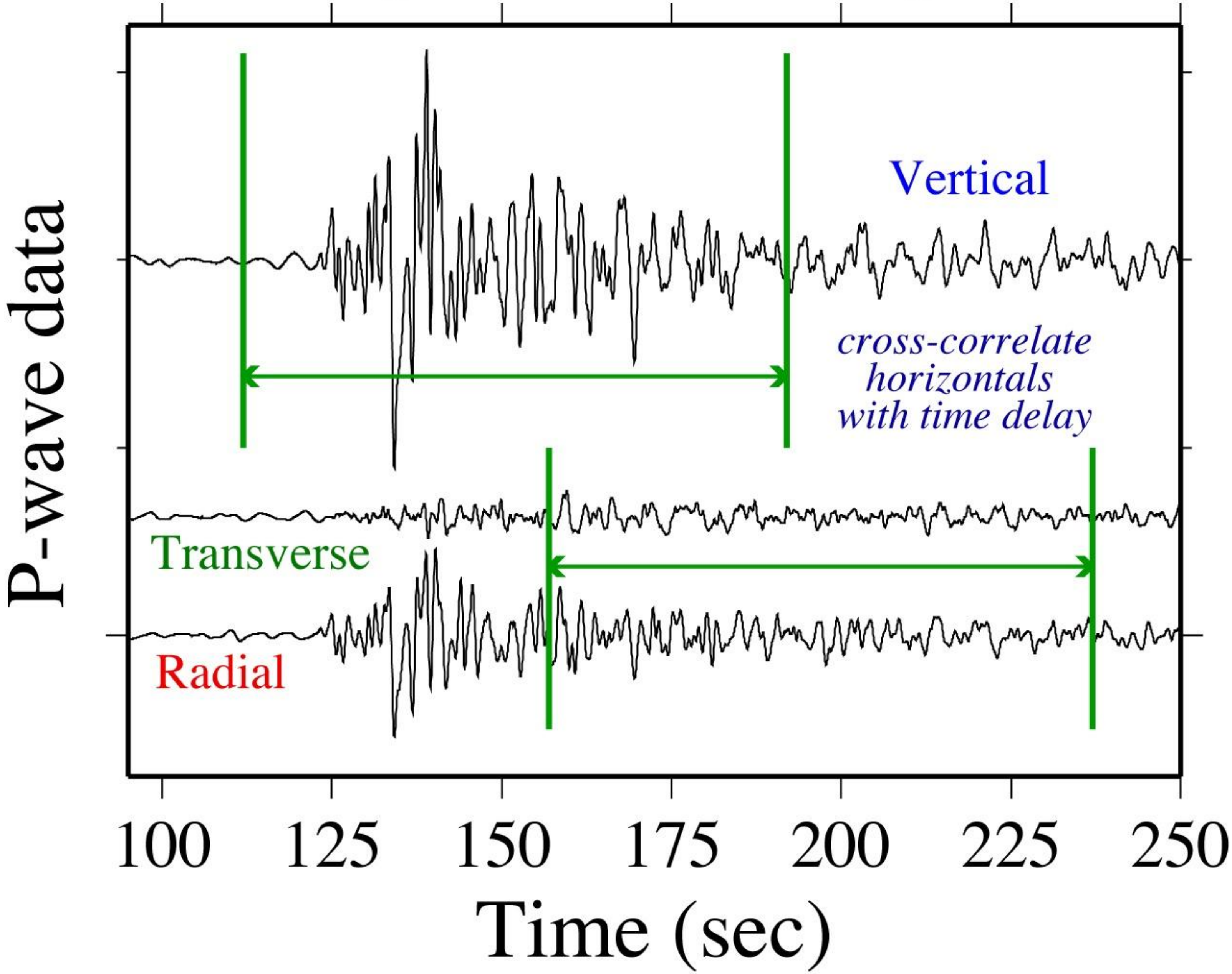

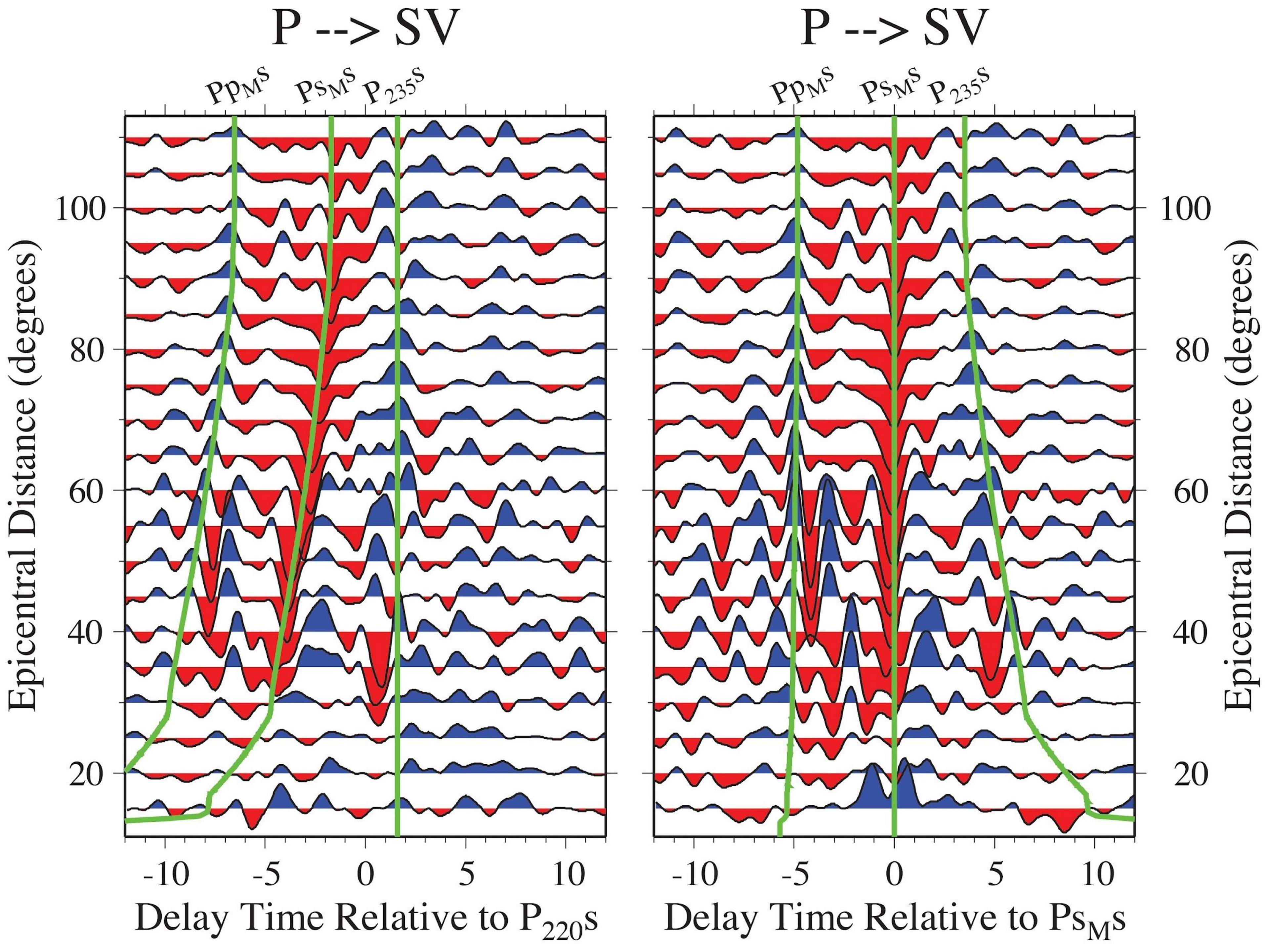

P --> SV
P --> SV
Pp_MS
Ps_MS
$P_{235}S$
Pp_MS
Ps_MS
$P_{235}S$
Epicentral Distance (degrees)
Epicentral Distance (degrees)
20
40
60
80
100
-10
-5
0
5
10
Delay Time Relative to $P_{220}s$
Delay Time Relative to Ps_Ms

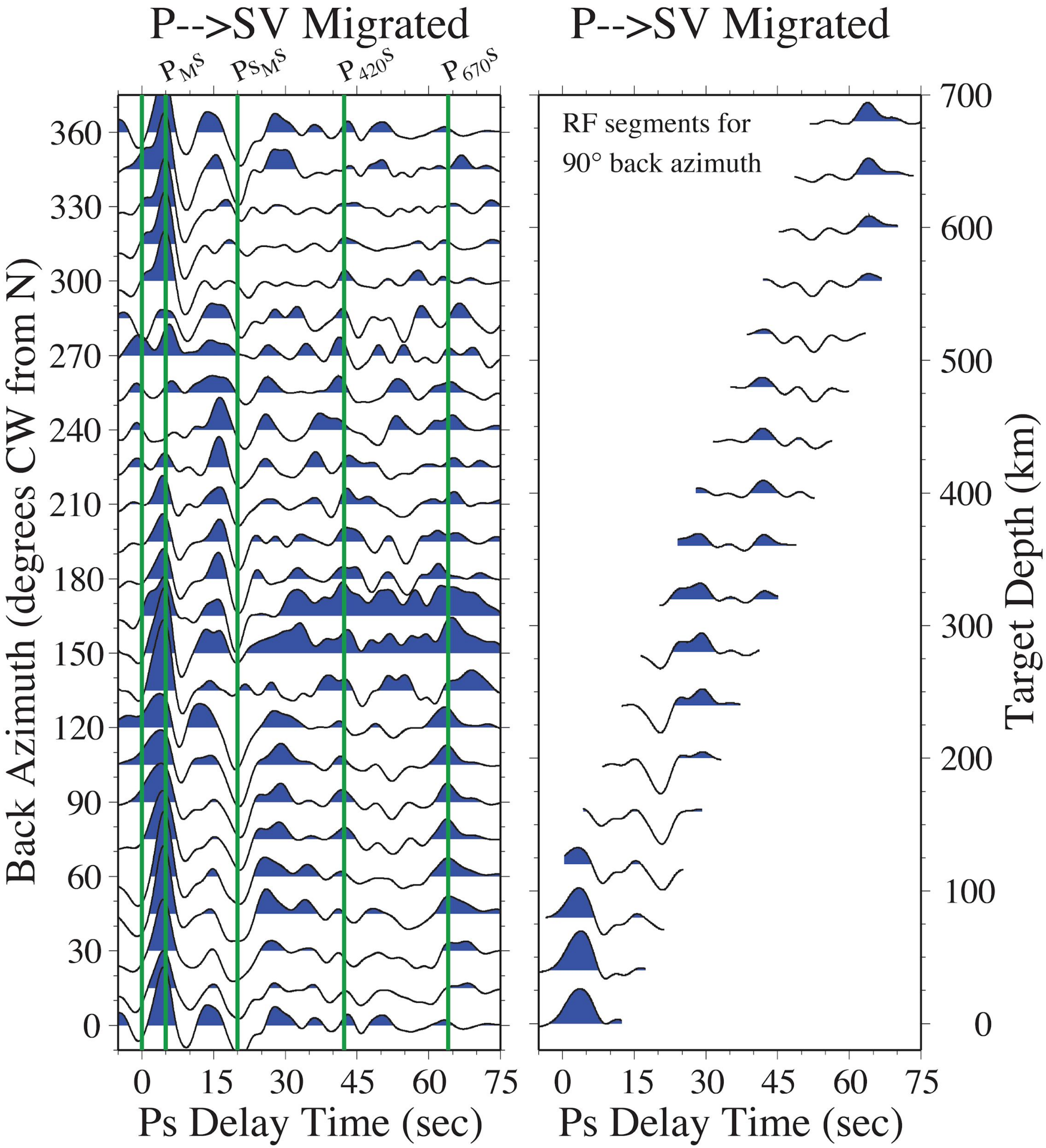

P-->SV Migrated
P-->SV Migrated
P_MS
Ps_MS
$P_{420}S$
$P_{670}S$
RF segments for
90° back azimuth
Back Azimuth (degrees CW from N)
Target Depth (km)
Ps Delay Time (sec)
Ps Delay Time (sec)

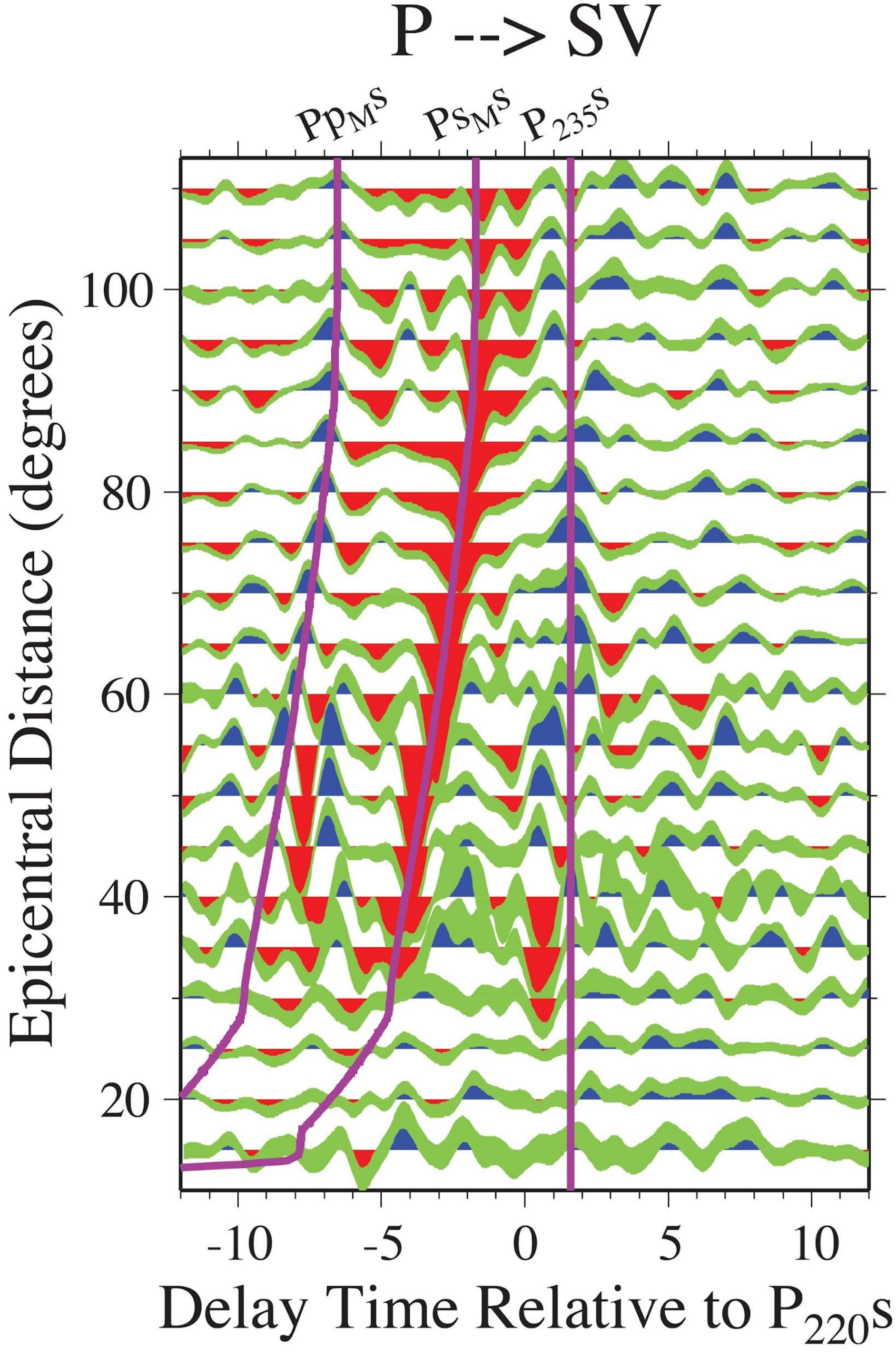

P --> SV
PpMS
PsMS
P235S
Epicentral Distance (degrees)
100
80
60
40
20
-10
-5
0
5
10
Delay Time Relative to P220s

Geophys. J. Int. (2016) **207**, 1216–1243
Advance Access publication 2016 August 26
GJI Seismology

doi: 10.1093/gji/ggw323

Anisotropic shear zones revealed by backazimuthal harmonics of teleseismic receivers functions

J. Park[1] and V. Levin[2]

[1]*Department of Geology and Geophysics, Yale University, New Haven, CT 06511, USA. E-mail: jeffrey.park@yale.edu*
[2]*Department of Geological Sciences, Rutgers University, Piscataway, NJ 08854, USA*

Accepted 2016 August 24. Received 2016 August 23; in original form 2016 March 25

Backus (1965) parameters for wavespeeds

$$\rho\alpha^2(\xi) = A + B\cos 2\xi + C\cos 4\xi$$

$$\rho\beta^2(\xi) = D + E\cos 2\xi .$$

ξ is the angle between wave propagation and symmetry axis

φ is the strike of symmetry axis
ψ is the tilt of symmetry axis

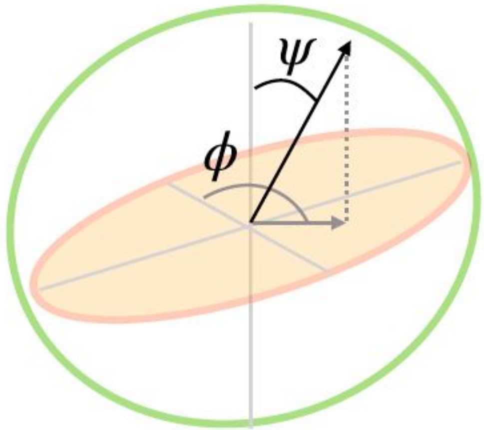

Figure 2
Conventions for angles ψ (tilt from vertical) and ϕ (strike clockwise from N) that describe the orientations of a symmetry axis

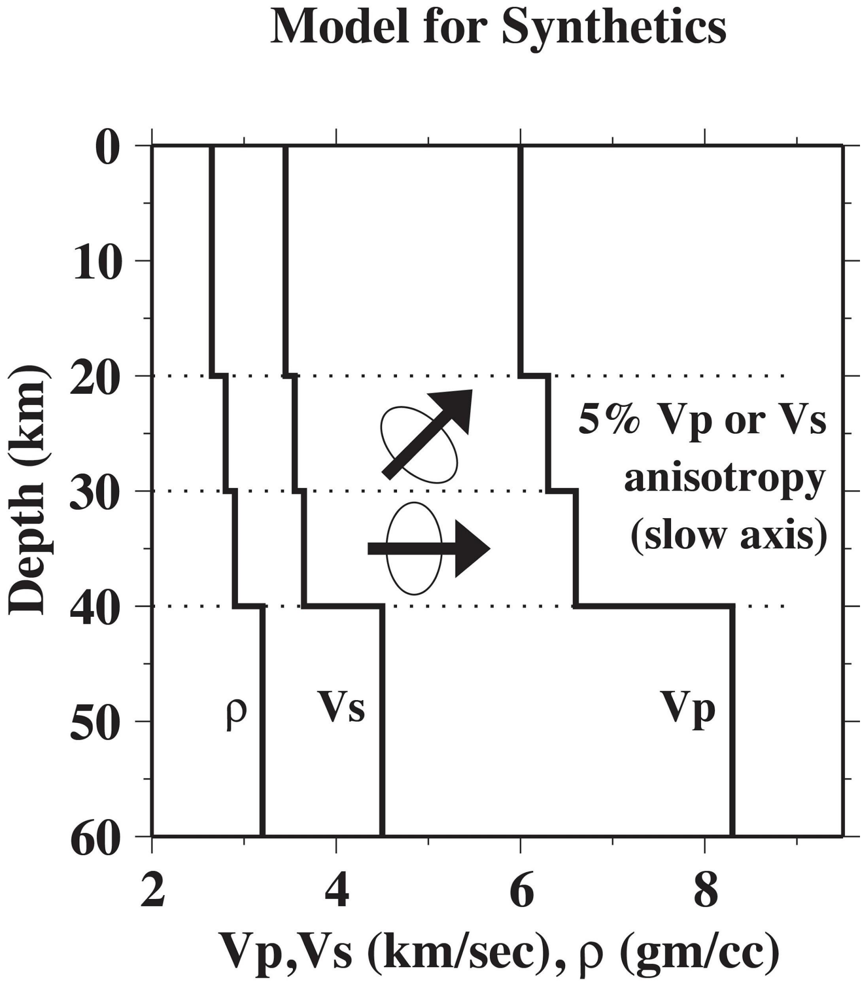

Test model with tilted-axis in middle crust, horizontal symmetry axis in lower crust

Compute synthetic receiver functions for 471 events at GSN Station RAYN (Ar Rayn, Saudi Arabia)

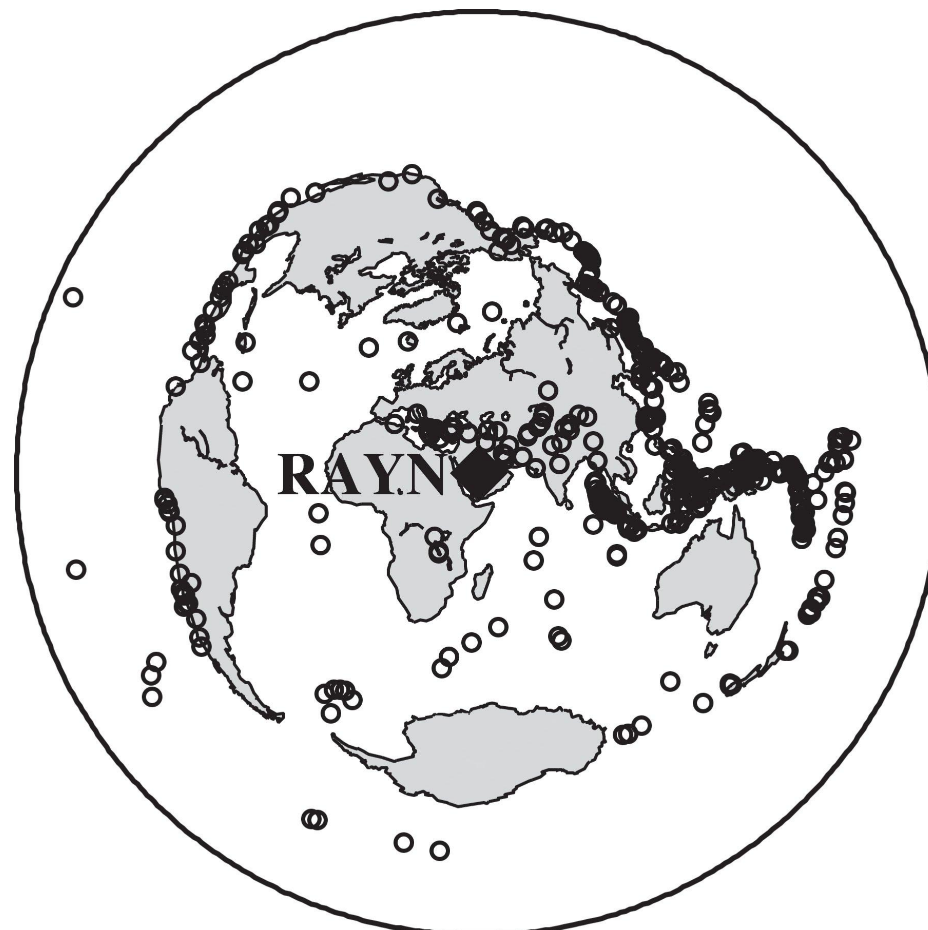

Synthetic RFs for events in 10° bins of back-azimuth are stacked in the freq domain

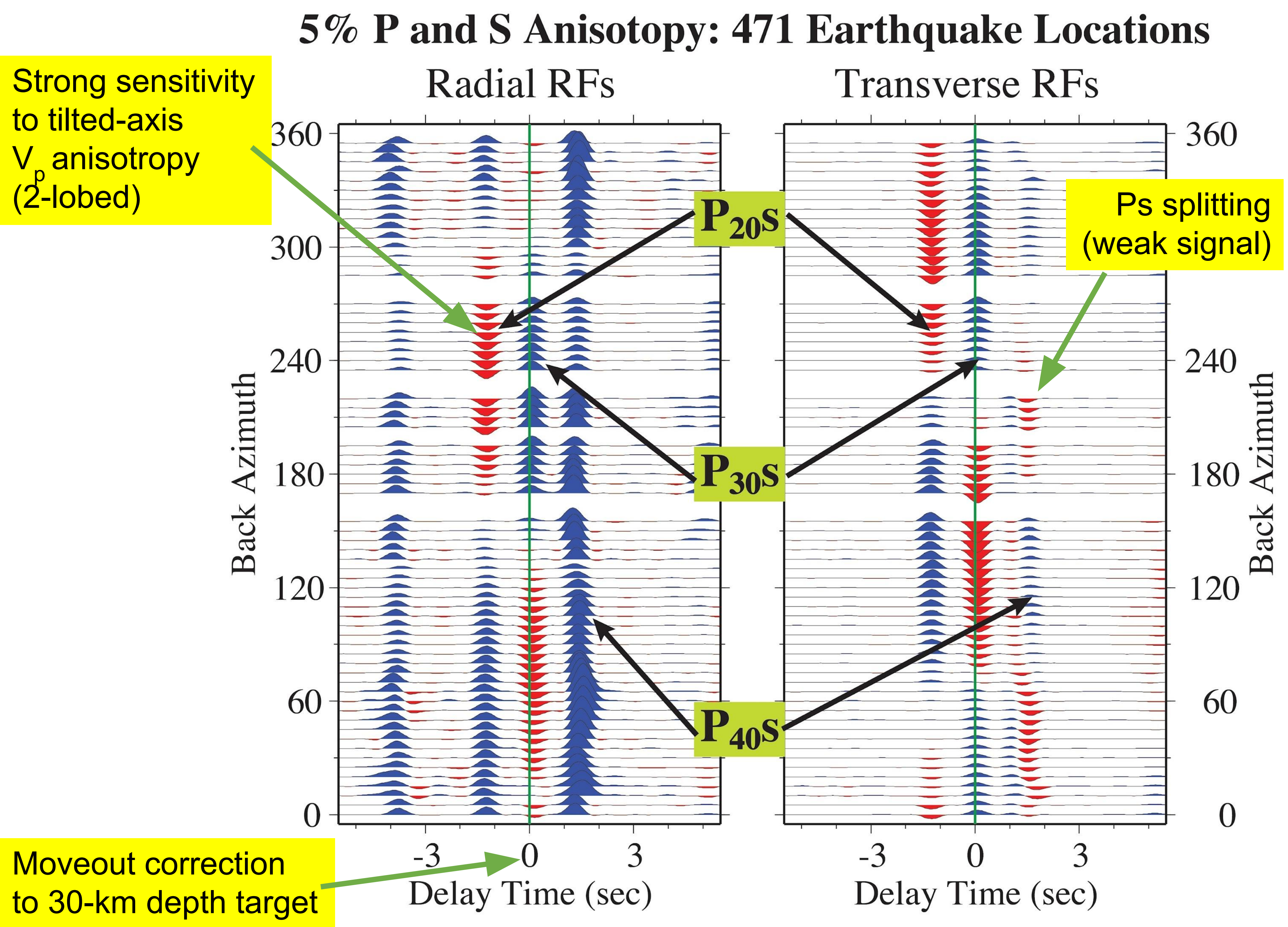

5% P and S Anisotopy: 471 Earthquake Locations
Radial RFs
Transverse RFs
Strong sensitivity to tilted-axis V_p anisotropy (2-lobed)
Ps splitting (weak signal)
$P_{20}s$
$P_{30}s$
$P_{40}s$
Moveout correction to 30-km depth target
Back Azimuth
Delay Time (sec)
360
300
240
180
120
60
0
-3
3

5% P and S Anisotopy: 471 Earthquake Locations

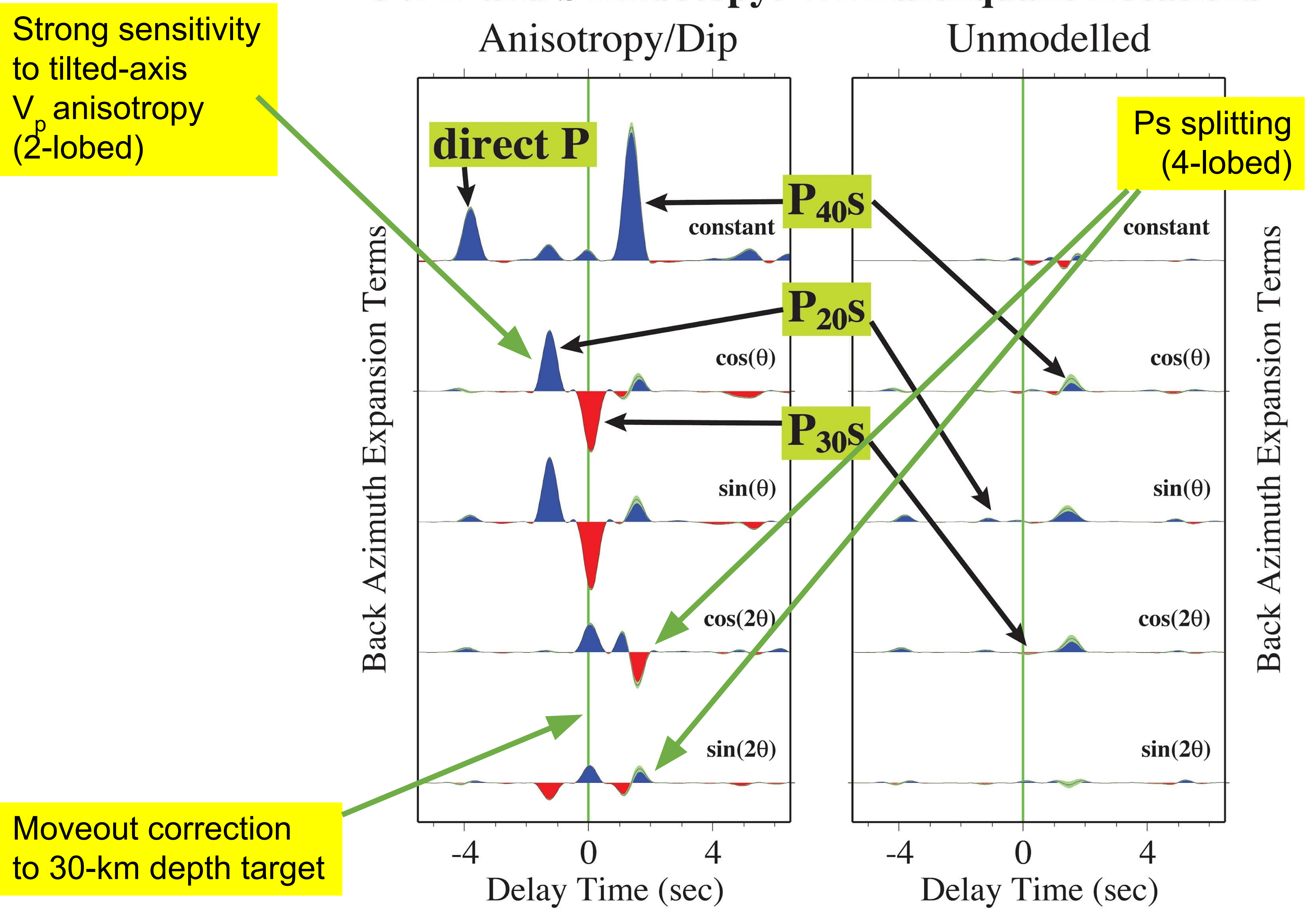

5% S Anisotopy Throughout Crust: Ps Splitting Test

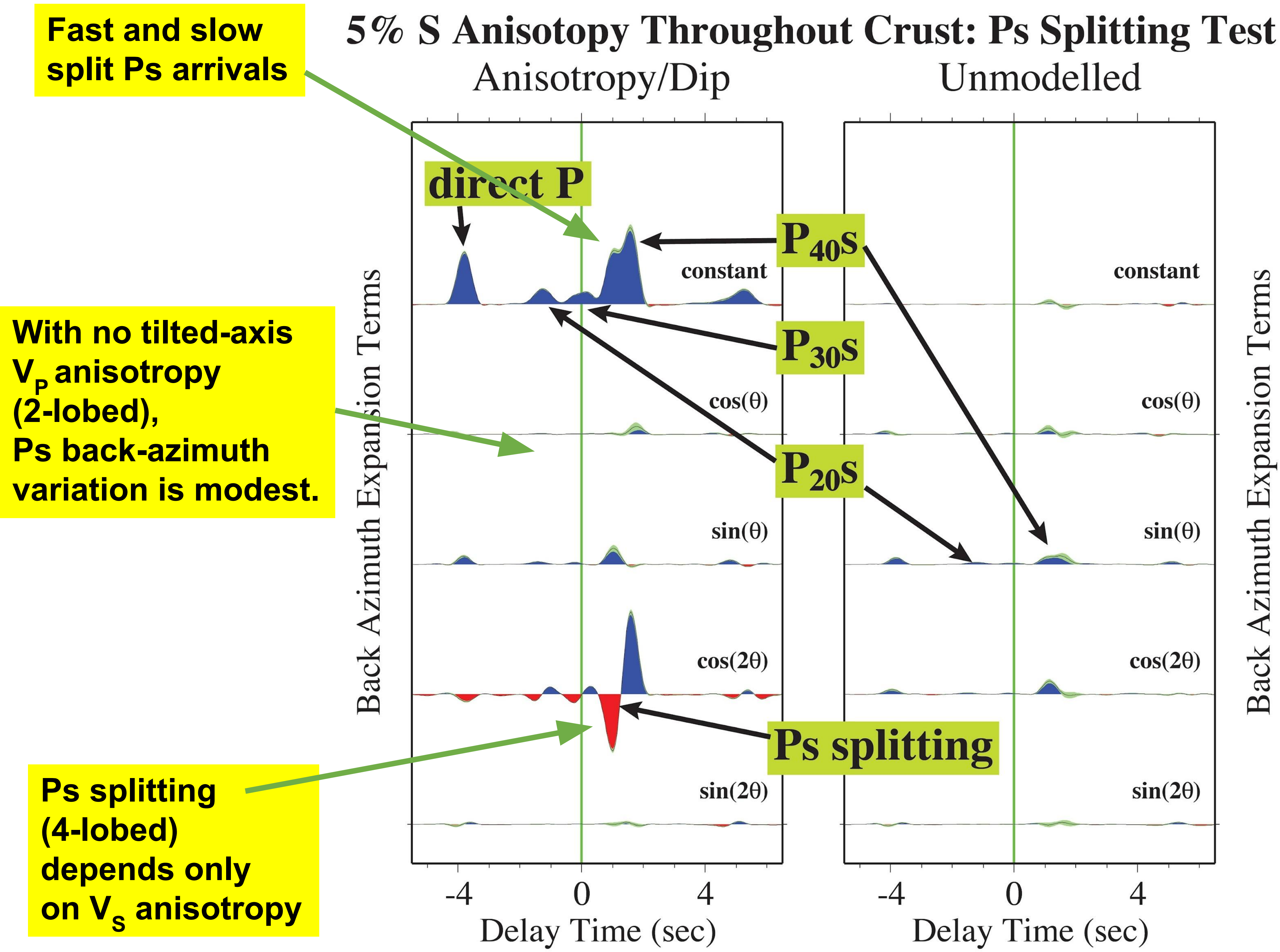

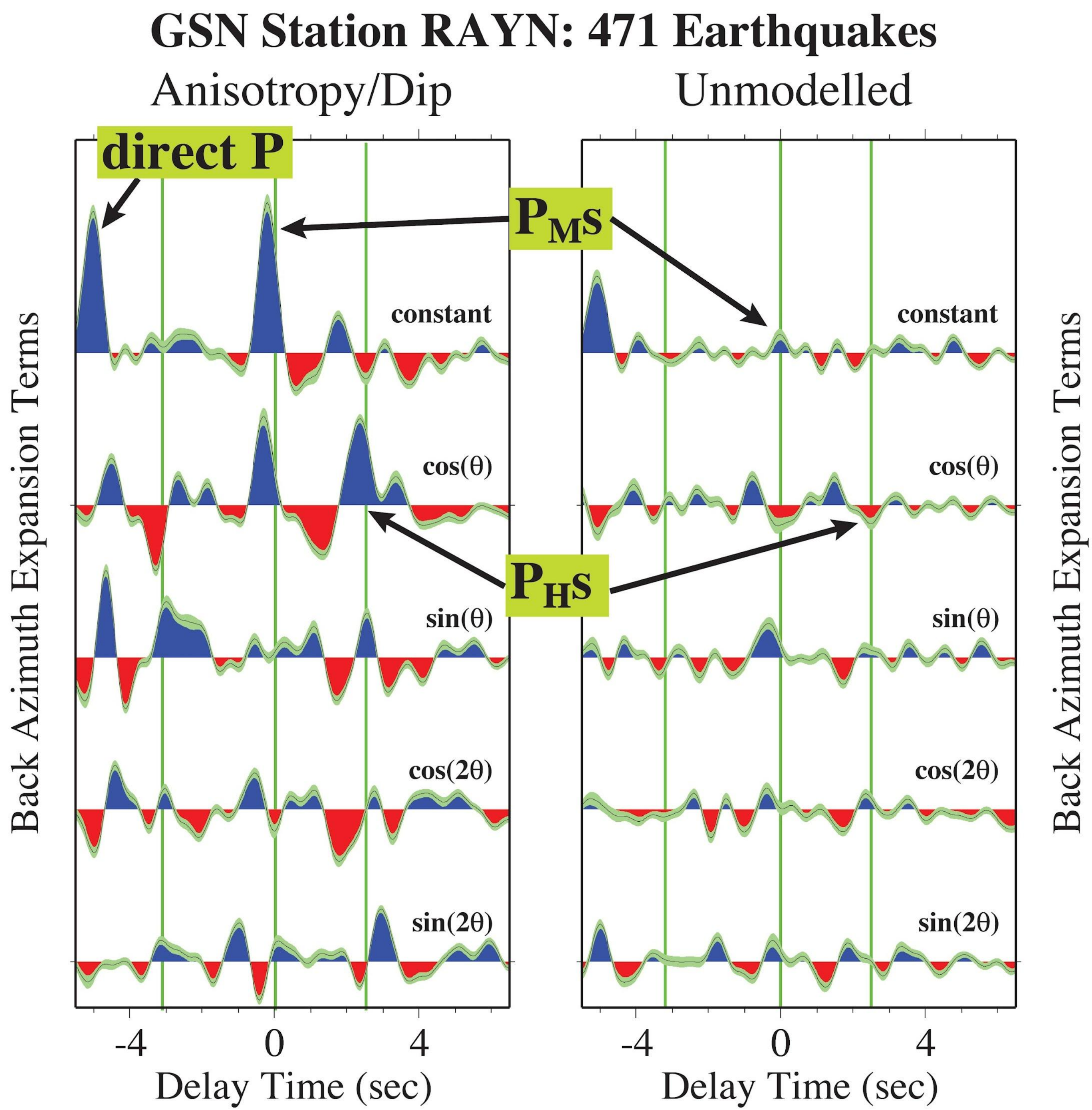

GSN Station RAYN: 471 Earthquakes
Anisotropy/Dip
Unmodelled
direct P
P_MS
P_HS
constant
cos(θ)
sin(θ)
cos(2θ)
sin(2θ)
constant
cos(θ)
sin(θ)
cos(2θ)
sin(2θ)
Back Azimuth Expansion Terms
Back Azimuth Expansion Terms
-4
0
4
-4
0
4
Delay Time (sec)
Delay Time (sec)

Geophysical Journal International

Geophys. J. Int. (2017) **208,** 1332–1341
doi: 10.1093/gji/ggw455
Advance Access publication 2016 December 7
GJI Seismology

Seismic receiver function interpretation: *P*s splitting or anisotropic underplating?

Zhen Liu and Jeffrey Park

Department of Geology and Geophysics, Yale University, New Haven, CT, USA. E-mail: z.liu@yale.edu

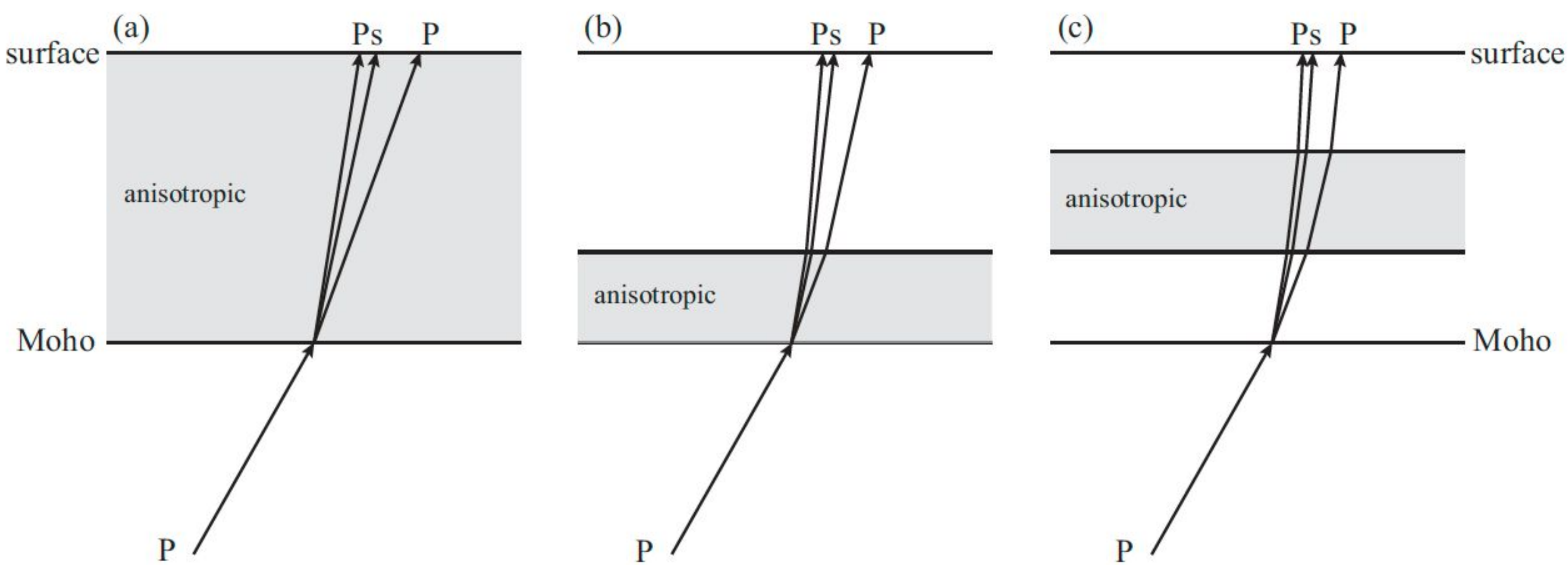

Figure 1. Shear wave splitting of Moho *P*s phases can be explained by the three crustal models shown above: (a) uniformly anisotropic crust; (b) anisotropic underplating at the base of crust; (c) mid-crustal anisotropic layering.

GSN Station ARU (Arti, Russia), near Urals-Mtns Suture

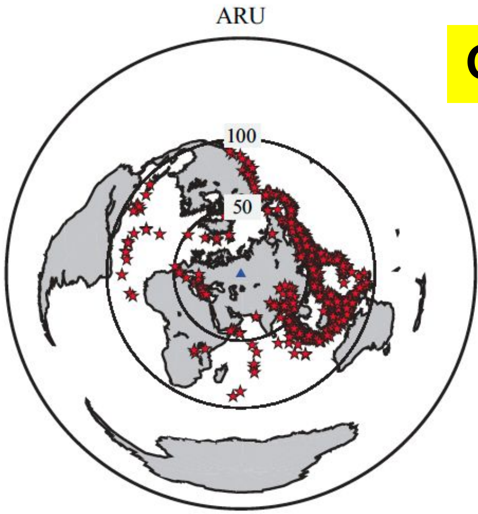

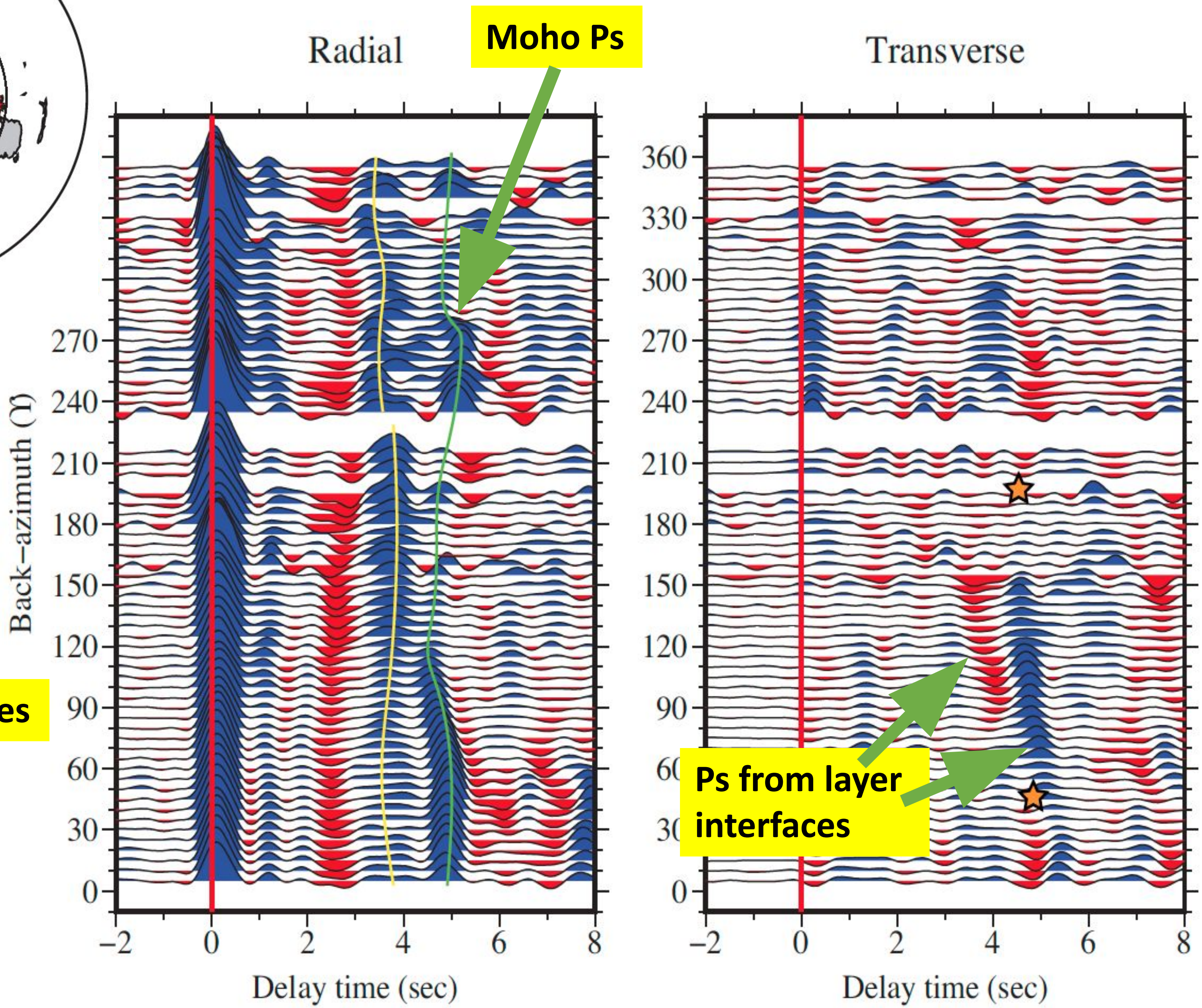

GSN Station ARU: Short-Period RFs

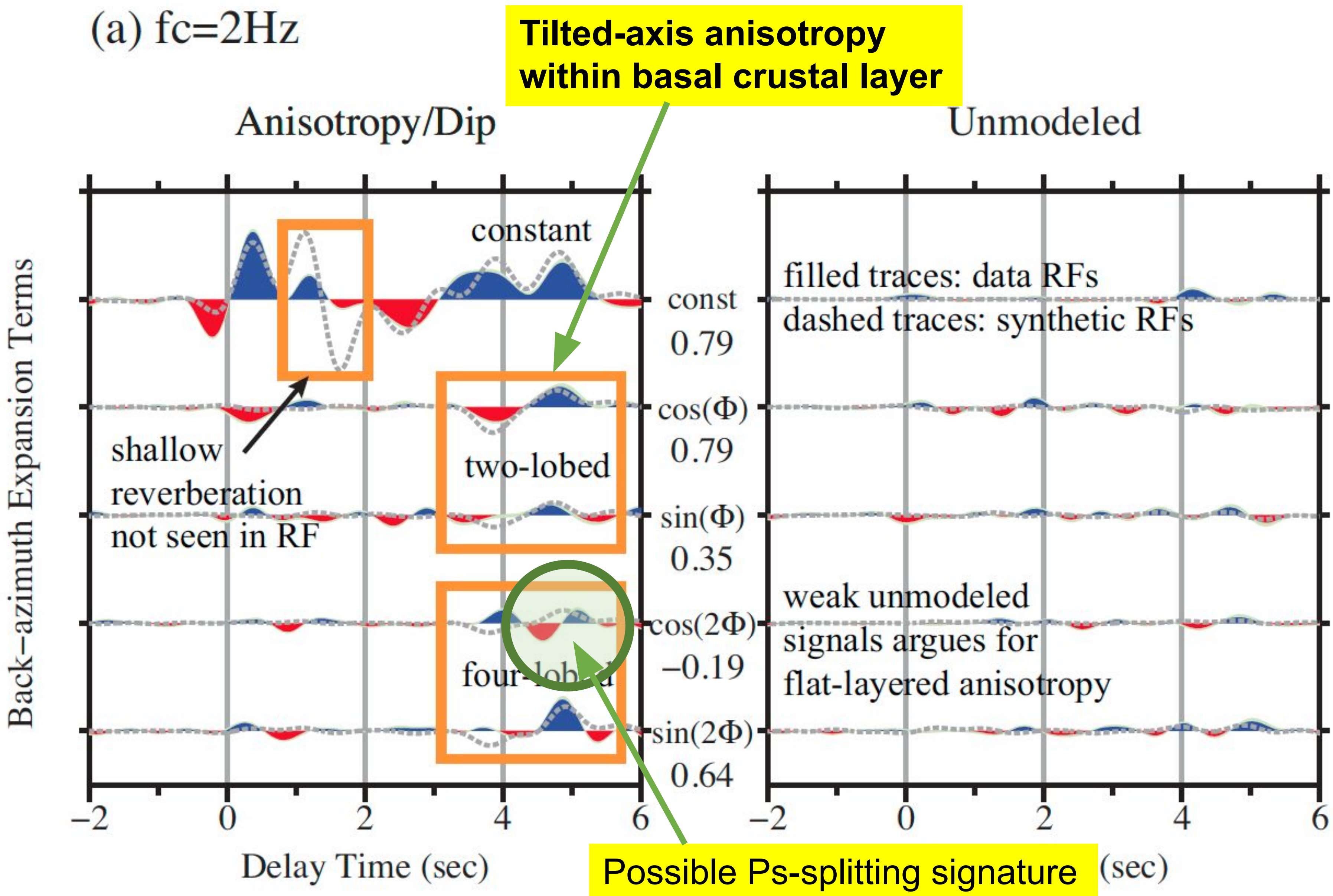

GSN Station ARU: Long-period RFs

(b) fc=0.5Hz

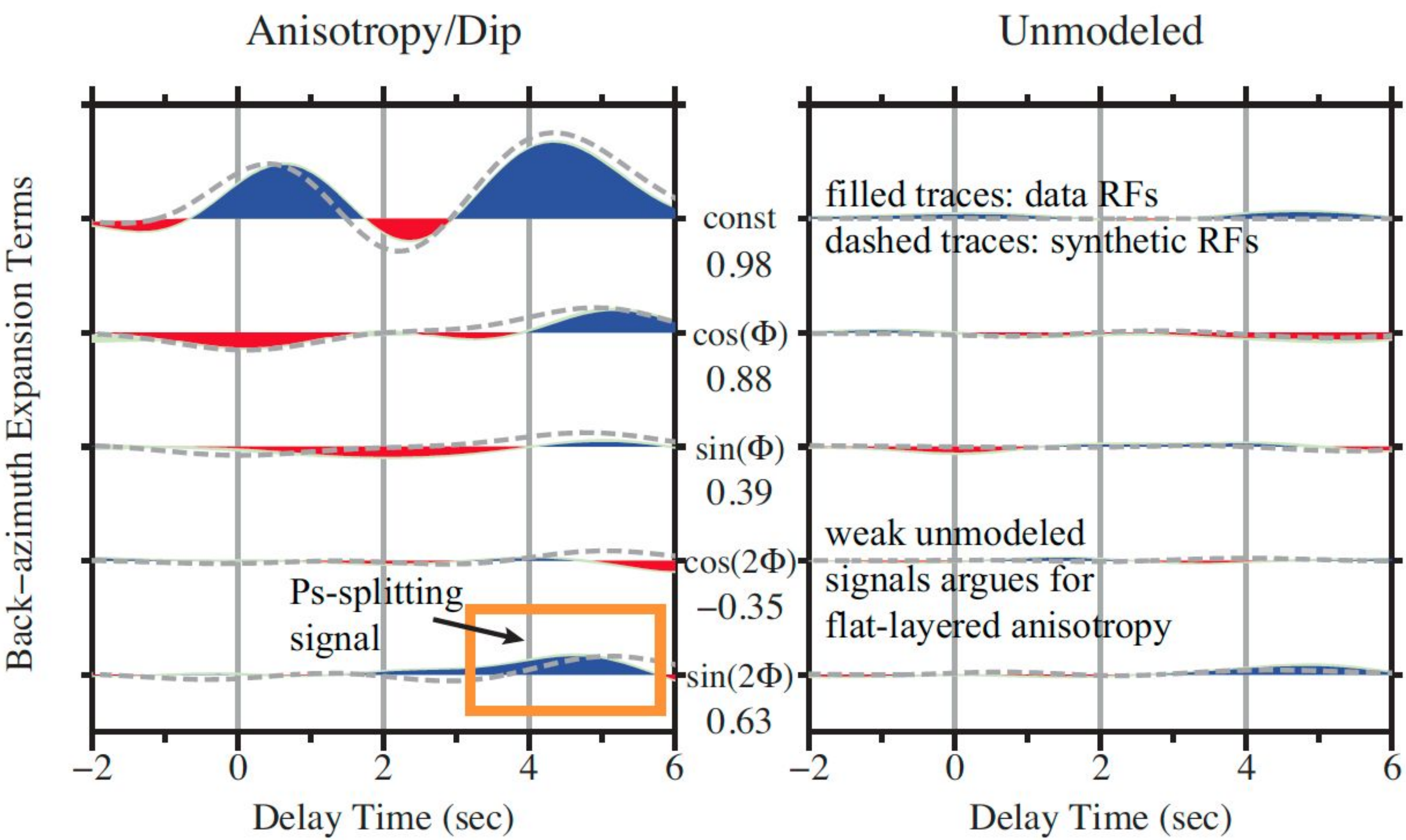

Crustal Velocity/Anisotropy Models for GSN Station ARU

Short Period:
Shear zone underlies
Low-velocity zone

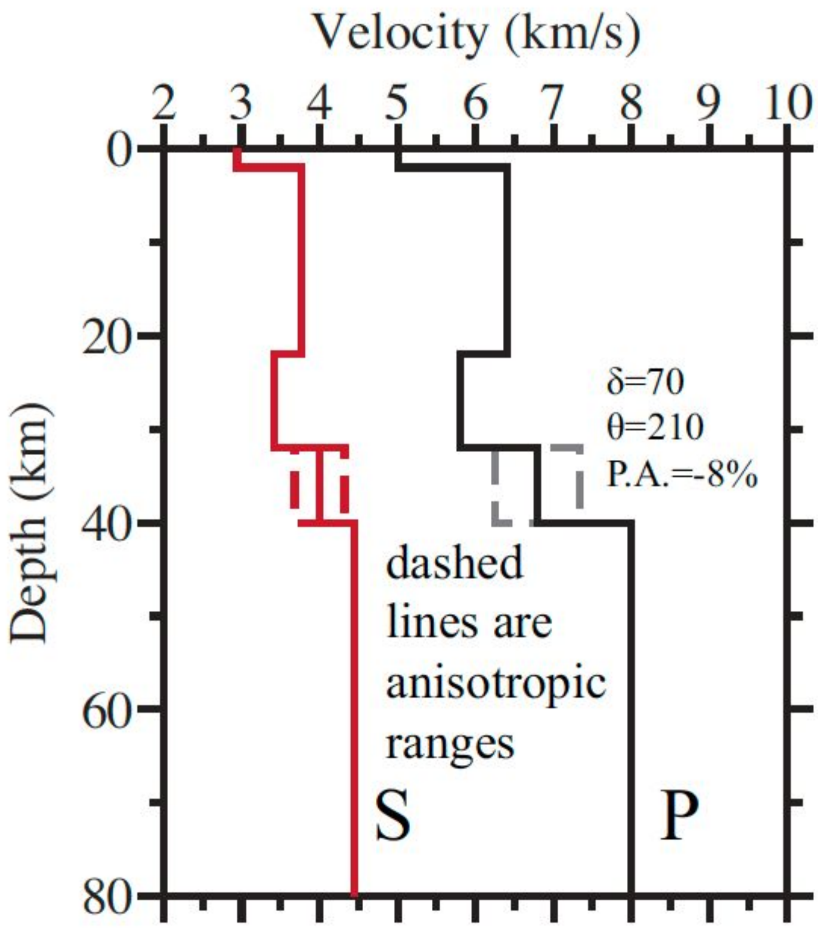

Long Period:
Shear zone not localized
LVZ weakly constrained

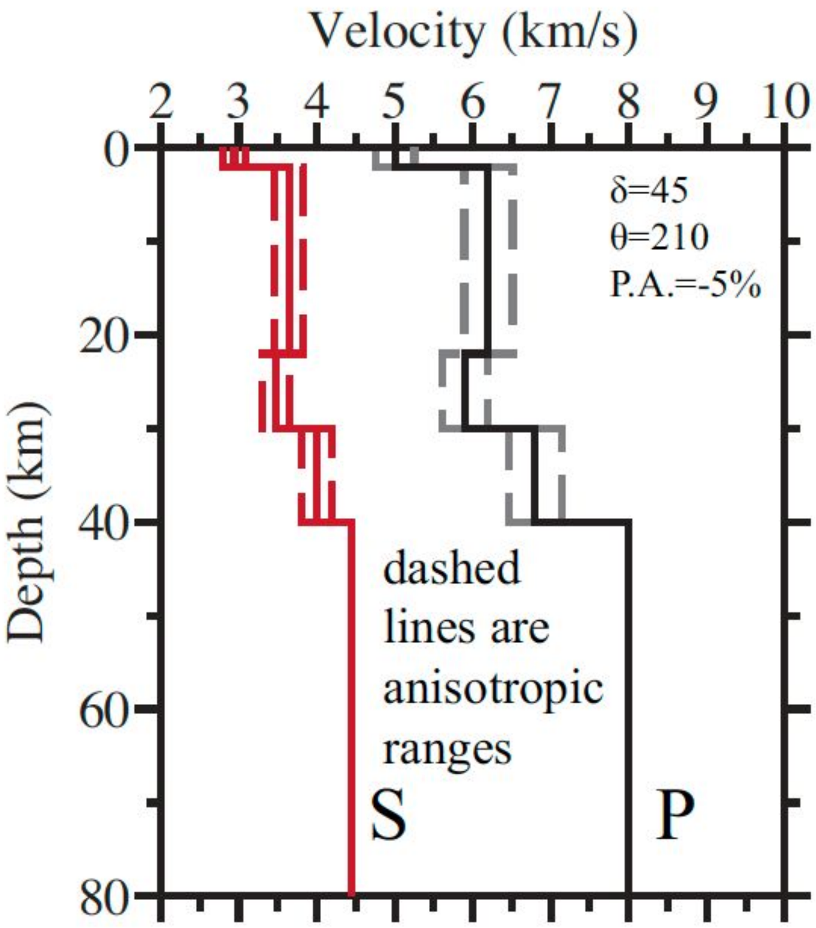

- We have developed a frequency-domain RF inversion algorithm using multiple-taper correlation (MTC) estimates, instead of spectral division, using the pre-event noise spectrum for frequency-dependent damping.

- The multi-taper spectrum estimates are leakage resistant, so low-amplitude portions of the P-wave spectrum can contribute usefully to the RF estimate.

- The coherence between vertical and horizontal components can be used to obtain a frequency-dependent uncertainty for the RF.

- The MTC method appears to be superior to two popular methods for RF-estimation, time-domain deconvolution (TDD) and spectral division (SPD), even if these are damped to avoid numerical instabilities.

Comments on Crustal Anisotropy:

- V_P anisotropy has stronger influence on Ps and Sp converted waves than does V_S anisotropy

- A tilted axis of symmetry generates larger Ps and Sp waves than a horizontal symmetry axis, particularly for near-vertical incidence.

- Sheared layers with the crust are common, but are better to isolate with short-period Ps receiver functions than with Ps birefringence.

- Gradual gradients of anisotropy within 5-20-km shear zones have characteristic signatures in RF back-azimuth sweeps and may be detectable in data

- Sp converted-wave amplitudes have harmonic dependence on back azimuth and may be useful in constraining anisotropy at sheared interfaces and sharp gradients within the mantle and even the crust, if high-frequency data can be obtained across full range of back-azimuth.

References

- Backus, G. E. (1965). Possible forms of seismic anisotropy of the uppermost mantle under oceans. **J. Geophys. Res., 70(14),** 3429–3439, doi:10.1029/JZ070i014p03429.
- Chen, X., J. Park and V. Levin, Anisotropic layering and seismic body waves: Deformation gradients, initial S-polarizations, and converted-wave birefringence, **Pure Appl. Geophys**, **178,** 2001–2023, doi:10.1007/s00024-021-02755-6, 2021.
- Langston, C.A., 1981. Evidence for the subducting lithosphere under southern Vancouver Island and western Oregon from teleseismic P wave conversions, **J. Geophys. Res., 86**, 3857–3866.
- Levin, V., and J. Park, Crustal anisotropy beneath the Ural mountains foredeep from teleseismic receiver functions, **Geophys. Res. Letts, 24**, 1283-1286, doi:10.1029/97GL51321, 1997**.**
- Liu, Z., and J. Park, Seismic receiver function interpretation: Ps splitting or anisotropic underplating?, **Geophys. J. Int**., **208,** 1332–1341, doi:10.1093/gji/ggw455, 2017.
- Park, J., and V. Levin, Receiver functions from multiple-taper spectral correlation estimates, **Bulletin of the Seismological Society of America**, **90**, 1507-1520, doi:10.1785/0119990122, 2000.
- Park, J., and V. Levin, Statistics and frequency-domain moveout for multiple-taper receiver functions, **Geophys. J. Int.**, **207**, 512-527, doi:10.1093/gji/ggw291, 2016.
- Park, J., and V. Levin, Anisotropic shear zones revealed by back-azimuthal harmonics of teleseismic receiver functions, **Geophys. J. Int**., **207**, 1216-1243, doi:10.1093/gji/ggw323, 2016.
- Park, J., C. R. Lindberg & F. L. Vernon III, Multitaper spectral analysis of high frequency seismograms, **J. Geophys. Res.**, **92**,12675-12684, 1987.
- Phinney, R.A., 1964. Structure of the Earth's crust from spectral behavior of long-period body waves, **J. Geophys. Res., 69**, 2997–3017.